Marine Geology 403 (2018) 301–328

Contents lists available at ScienceDirect

Marine Geology

journal homepage: www.elsevier.com/locate/margo

The Central Paratethys during Oligocene as an ancient counterpart of the present-day Black Sea: Unique records from the coccolith limestones

Maciej J. Bojanowski[a,*], Agnieszka Ciurej[b,c], Grzegorz Haczewski[b], Petras Jokubauskas[d], Stefan Schouten[e,g], Jarosław Tyszka[b], Peter K. Bijl[f]

[a] ING PAN - Institute of Geological Sciences, Polish Academy of Sciences, Twarda 51/55, 00-818 Warszawa, Poland
[b] ING PAN - Institute of Geological Sciences, Polish Academy of Sciences, Research Centre in Cracow, Senacka 1, 31-002 Kraków, Poland
[c] Institute of Geography, Pedagogical University of Cracow, Podchorążych 2, 30-084 Kraków, Poland
[d] Institute of Geochemistry, Mineralogy and Petrology, Faculty of Geology, University of Warsaw, Żwirki i Wigury 93, 02-089 Warszawa, Poland
[e] NIOZ Royal Netherlands Institute for Sea Research, Department of Marine Microbiology and Biogeochemistry, Landsdiep 4, 1797 SZ 't Horntje (Texel), the Netherlands
[f] Marine Palynology and Palaeoceanography, Laboratory of Palaeobotany and Palynology, Department of Earth Sciences, Faculty of Geosciences, Utrecht University, Princetonlaan 8A, 3584 CB Utrecht, the Netherlands
[g] Department of Earth Sciences, Faculty of Geosciences, Utrecht University, Budapestlaan 4, 3584 CD Utrecht, the Netherlands

ARTICLE INFO

Keywords:
Pelagic sediments
Marginal basins
Paleoceanography
Salinity
Redox conditions
Methane venting

ABSTRACT

Four isochronous Oligocene coccolith limestone horizons from the Carpathians were examined in order to reconstruct paleoceanographic conditions in the Central Paratethys. The dominance of small and size-uniform pyrite framboids, the occurrence of low-diversity dinoflagellate cysts and coccolithophorids and the presence of biomarker molecule 28,30-dinorhopane indicate that the water column was stratified with the upper water column being relatively well-oxygenated, but the bottom water being anoxic. The latter is confirmed by the fine and consistent horizontal laminations in various parts of the basin, scarcity of benthic organisms and their trace fossils. The limestones exhibit typical marine $\delta^{13}C$ values, but are significantly depleted in ^{18}O and enriched in ^{87}Sr relative to contemporaneous ocean water. These isotopic compositions result from a decreased salinity of the surface waters caused by an increased riverine input. This is confirmed by the lack or impoverishment of planktonic foraminifers, presence to abundance of goniodomid dinoflagellate cysts and massive occurrence of low-diversity nannoplankton assemblages, which indicates decreased salinities as low as 17‰ and high productivity in the upper water column. These observations indicate that the limestones were formed during periods when connection of the Central Paratethys with the global ocean was limited, which impeded water exchange causing the development of low-salinity conditions of surface water and bottom-water anoxia. During the deposition of the oldest Tylawa horizon, primary productivity was enhanced and chemocline was positioned exceptionally high in the water column. Moreover, decreased $\delta^{13}C$ values in both carbonates and organic matter of this horizon suggest that widespread methane venting took place in the basin during NP23. All these data show that during the Oligocene the Central Paratethys experienced similar conditions to those of the current Black Sea, which can be used as a modern analogue, especially for the Tylawa horizon. Therefore, the Tylawa horizon can be perceived as a potential effect of future post-depositional processes of coccolith marls analogous to those having been deposited in the Black Sea for 2.7 kyr.

1. Introduction

Large marginal basins having limited connections with the ocean provide unique settings for reconstructing past paleoceanography and climate, as they are susceptible to even subtle variations of global (e.g. eustatic) and regional (e.g. tectonic) phenomena. The sedimentary infills of such basins provide a valuable archive of these variations manifested in depositional, biotic and geochemical proxies that quickly and distinctly respond to changes of sea-level, water circulation, temperature, salinity, nutrient supply, redox conditions, riverine input etc. The Black Sea is currently the largest anoxic marginal basin on Earth. A weak connection with the Mediterranean and a large input of riverine water produce brackish conditions. The water column is stratified with respect to both O_2 concentration and salinity (Codispoti et al., 1991;

* Corresponding author.
E-mail addresses: mbojan@twarda.pan.pl (M.J. Bojanowski), aciurej@up.krakow.pl (A. Ciurej), p.jokubauskas@student.uw.edu.pl (P. Jokubauskas), stefan.schouten@nioz.nl (S. Schouten), ndtyszka@cyf-kr.edu.pl (J. Tyszka), p.k.bijl@uu.nl (P.K. Bijl).

https://doi.org/10.1016/j.margeo.2018.06.011
Received 14 August 2017; Received in revised form 7 June 2018; Accepted 19 June 2018
Available online 27 June 2018
0025-3227/

Tuğrul et al., 1992) and anoxia reaches as high as the euphotic zone (< 100 m) in the distal parts (> 2000 m water depth) (Huang et al., 2000). This situation boosts primary productivity in the euphotic zone, which is mainly manifested by massive, seasonal coccolithophore blooms of *Emiliana huxleyi* (Eker-Develi and Kideys, 2003), and enhances the preservation of organic matter being transported to the seafloor (Calvert and Karlin, 1998; Stewart et al., 2007). As a consequence, micro-laminated coccolith- and organic C-rich sediments interspersed with dark fine-grained turbidites are deposited in the deep parts of the basin (Lyons, 1991; Arthur and Dean, 1998). Highly reducing conditions and high C_{org} content enable widespread methane production in the sediments (Reeburgh et al., 1991). Methane is liberated into the water column by fluid seepage (Peckmann et al., 2001; Thiel et al., 2001; Michaelis et al., 2002) where it is effectively being oxidized, mainly via anaerobic oxidation (Schouten et al., 2001; Wakeham et al., 2003).

Several authors have suggested that paleoceanographic conditions in Paratethys during the Oligocene, i.e. water-column stratification and low-salinity conditions in a restricted basin, were analogous to those in the present-day Black Sea (Báldi, 1984; Haczewski, 1989; Schulz et al., 2005; Sótak, 2010). The Paratethys was one of the seas that originated from the decay of the Tethys Ocean at the end of the Eocene (Báldi, 1984; Rögl, 1998). It was bordered to the south by rising collisional orogens and consisted of a series of marine basins whose extents, depths, mutual connections and connections with adjacent ocean basins were constantly changing. Fluctuations in sea-level, salinity, temperature and nutrient supply have been used to explain the alternating deposition of turbidites, organic C-rich mudstones, diatomites and coccolith limestones in the Paratethys (Rögl, 1998, 1999; Schulz et al., 2005; Sótak, 2010). A stratified water column, with stagnating bottom water and normal salinity with episodes of freshening near the sea surface, have been proposed to have occurred during deposition of organic C-rich mudstones (Vetö, 1987; Rögl, 1998, 1999; Melinte, 2005), which are important source rocks for oil and gas in the Alpine foreland, Carpathians and the Caspian Sea regions (Köster et al., 1998a; Schulz et al., 2005; Schmidt and Erdogan, 1996). Organic geochemical analyses of these rocks (Köster et al., 1998a, 1998b; Schulz et al., 2005) indicated that anoxicity reached even as high as the photic zone. The most comprehensive comparison between the Paratethys during Oligocene and present-day Black Sea was performed by Schulz et al. (2005). However, they studied the Dynów Marls, which are not the best possible Oligocene Paratethyan counterpart of the currently deposited laminated coccolith ooze in the Black Sea, as they lack the distinctive regular, fine lamination. Moreover, important paleoceanographic phenomena that take place in the Black Sea, i.e. methane seepage, anaerobic oxidation of methane, microbial sulfate reduction, were either not discussed or not verified for the Oligocene Paratethyan deposits in these studies. Thus, a reliable and systematic comparison between the Oligocene Paratethys and present-day Black Sea is needed, which is the scope of this work.

While the great majority of studies on the paleoenvironment of the Paratethys was based on investigations of the laterally variable and strongly diachronuous Oligocene facies, isochronous marker horizons traceable across the different facies zones and tectonic units should be central for studies on the sedimentary history of the Paratethys, as they represent a snapshot of paleoceanographic conditions in different and distant parts of the basin. The most useful among them are thin intervals of pelagic, finely laminated coccolith limestones, traceable over the whole Outer Carpathians and adjacent basins (Koszarski and Żytko, 1961; Jucha, 1969; Haczewski, 1989; Krhovský et al., 1992; Melinte, 2005; Schulz et al., 2005; Kotlarczyk et al., 2006). They occur as distinct thin interbeds within predominant siliciclastic gravity-flow deposits and organic C-rich shales. They were formed by intensive pelagic carbonate sedimentation induced by phytoplankton blooms within a large part of the Paratethys analogous of the recent Black Sea sediments. Krhovský et al. (1992), based mainly on the analysis of nannoplankton assemblages, maintained that during the deposition of the coccolith limestones, the basin was brackish for most of the time with only short episodes of salinity rising to near-normal marine values. Kotlarczyk et al. (2006) and Bieńkowska-Wasiluk (2010), based on the analysis of fish fauna, concluded that anoxia was intermittently present in the water column. Still, controversies exist concerning the specific paleoceanographic conditions that persisted in the basin and favored formation of these limestones (e.g. Haczewski, 1989; Krhovský et al., 1992; Ciurej, 2009).

The main purpose of this work is to constrain the paleoenvironmental conditions in the Central Paratethys at the time of the deposition of the coccolith limestones by a systematic examination of all four Oligocene horizons on a basin-wide scale employing a multiproxy approach. We have chosen a wide range of methods, i.e. examination of foraminifera and dinoflagellate cyst assemblages, measurements of pyrite framboid diameters, lipid biomarker analysis, isotopic analyses of C, O and Sr in carbonates, C and N in organic matter and S in framboidal pyrite, that are considered as robust and for which data exist from the current Black Sea and its recent sediments. The Black Sea is a particularly valuable natural laboratory in which many of these proxies have been in fact tested and calibrated for evaluating paleoenvironmental conditions. The data obtained in this study are discussed with respect to paleoceanographic reconstructions and point-by-point compared to the relevant major characteristics of the Black Sea today and its sediments deposited over the last 2.7 kyr.

2. Geological settings

The Oligocene coccolith limestones from different areas of the Outer Carpathians (22 sections: 18 from Poland, 4 from Romania) and from the Transylvanian Basin (one section) were examined (Fig. 1). The Oligocene deposits of the Outer Carpathians lie in the upper part of an Upper Jurassic-Lower Miocene sedimentary sequence folded and thrust in a pile of nappes onto the outer foredeep of the Carpathian orocline. Dark, organic C-rich shales intercalated with siliciclastic gravity mass-flow deposits are the most distinctive Oligocene facies. Two main facies zones are defined by clastic sediments predominating in volume over the dark shales: the outer zone with the Kliwa Sandstone supplied from the external margin of the basin and the inner zone with the Krosno Beds (equivalent to Fusaru Sandstone, Pucioasa Beds and Vineţişu Beds in Romania). The facies with the Krosno Beds appeared first in the internal parts of the basin and prograded outwards as is shown by the changing position of the limestone horizons relative to the major facies (Fig. 2). Two southernmost sections (Buciumeni and Suslăneşti) represent transitional zone between the outer nappes (the Skole-Tarcău unit) and the foreland (Puglisi et al., 2006). The Fântânele section in the Transylvanian Basin, on the rear side of the orocline, represents a sedimentary realm separated from the Outer Carpathian part of the Paratethys, but with the equivalents of the Outer Carpathian coccolith horizons.

Four coccolith limestone horizons are traced over the nearly whole length of the Outer Carpathians: Tylawa (TL-1), Jasło (JL-2), Sokoliska (SL-3) and Zagórz (ZL-4) limestones. Each horizon is isochronous, which makes them valuable chronostratigraphic markers in the Oligocene strata. TL-1 lies in the middle of the nannoplankton NP 23 zone (Krhovský et al., 1992; Melinte, 2005). Biostratigraphical positions of JL-2 and ZL-4 fall within the NP24 zone (Krhovský, 1981; Bąk, 2005; Melinte, 2005; Švábenická et al., 2007). Bąk (1999) placed ZL-4 in the foraminiferal zone P21, which is in agreement with an earlier work by Olszewska (1984). SL-3 lies between JL-2 and ZL-4, closer to the former, and thus also represents the NP24 zone (see also Ciurej and Haczewski, 2016). Therefore, JL-2, SL-3 and ZL-4 were laid down during the Rupelian-Chattian transition within merely a few tens of thousands years (Haczewski, 1989).

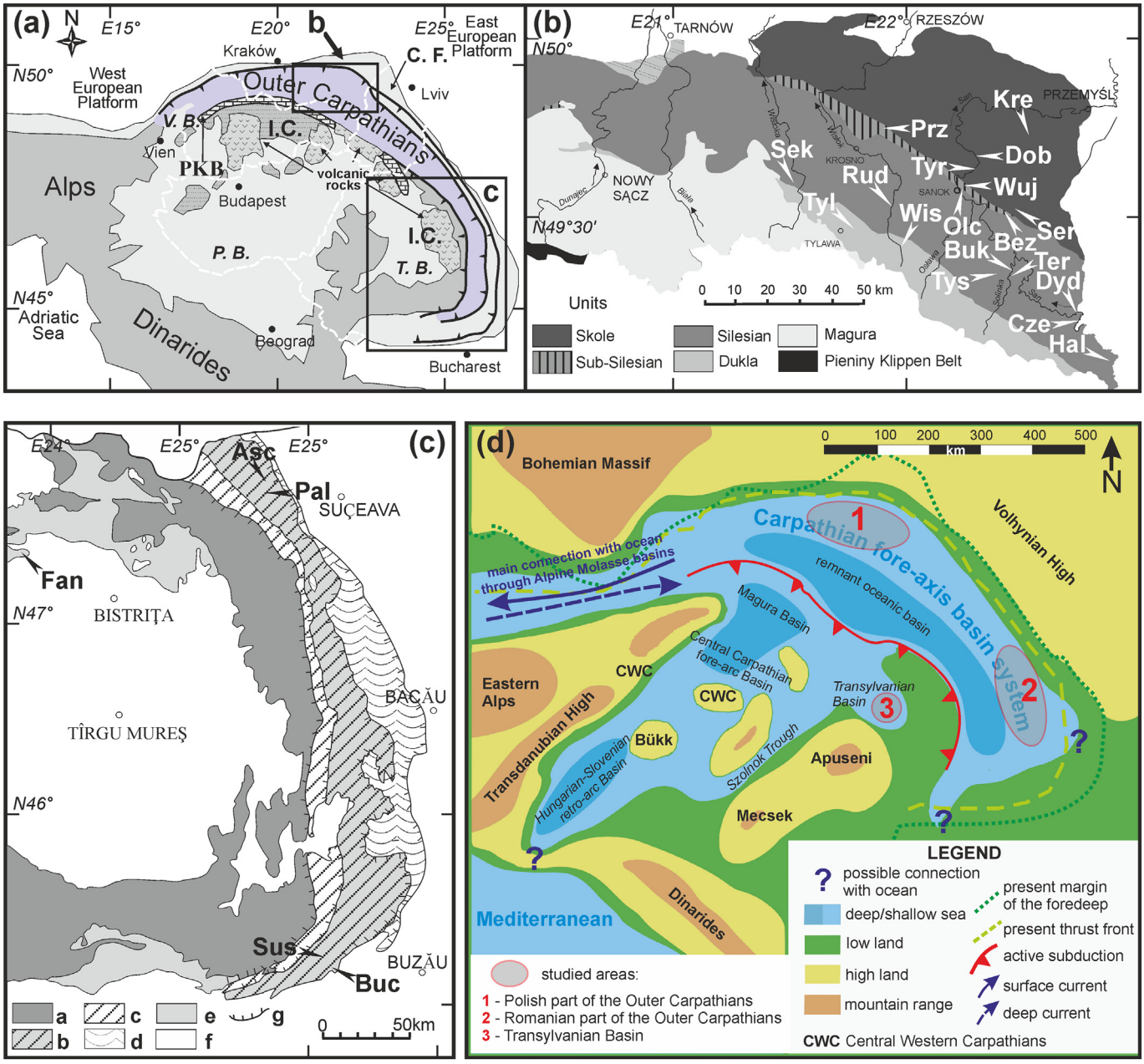

Fig. 1. Location maps and paleogeographic setting of the basins during Oligocene. (a) Simplified geological map of the Outer Carpathians with the location of the study areas (based on Kováč et al., 1998); C.F. - Carpathian Foredeep, I.C. - Inner Carpathians, P.B. - Pannonian Basin, PKB - Pieniny Klippen Belt, T.B. - Transylvanian Basin, V.B. - Vienna Basin. (b) Simplified geological map of the Polish part of the Outer Carpathians with locations of the sections. (c) Simplified geological map of the Romanian part of the Outer Carpathians with locations of the sections. Main tectonic units: a – Dacides (= Inner Carpathian units); b – Tarcău unit; c – inner Moldavide units; d – Marginal Folds unit; e – post-nappe cover, f - post-tectonic covers younger than Paleogene, g – major thrusts. (d) Setting of the Carpathian basins and the study areas on the paleogeographic map of the Paratethys sea for Late Rupelian, 32–29 Ma (Kováč et al., 2017, modified). Note the location of possible gateways for oceanic ingressions.

3. Material and methods

23 sections from Poland and Romania were examined; lithologic logs of three of them are depicted in Fig. 3. Details of locations, geological settings and lithologic logs of all sections are given in previously published work (e.g. Haczewski, 1989; Ciurej, 2009; Ciurej and Haczewski, 2012, 2016). Apart from limestones, intercalating mudstones were also sampled, mostly for palynological and organic geochemistry analyses (Table 1). Technical details of the methods described below are given in the Appendix.

3.1. Petrographic and micropaleontological investigations

Meso- and microtextural examination was performed on the vertical polished sections of all limestone samples. 90 thin sections were studied under a Zeiss Axioskop 50 polarizing microscope. Selected 56 thin sections were analyzed under scanning electron microscopes (SEM) equipped with energy-dispersive spectrometer (EDS). Measurements of pyrite framboid sizes were performed on 24 uncovered thin sections using a SEM (Zeiss Σigma VP SEM-FE). We developed an original procedure for automatic identification of framboidal pyrite and measurement of their sizes using the Esprit 1.9 software (see Appendix for details). The distribution of framboid diameters was analyzed on the basis

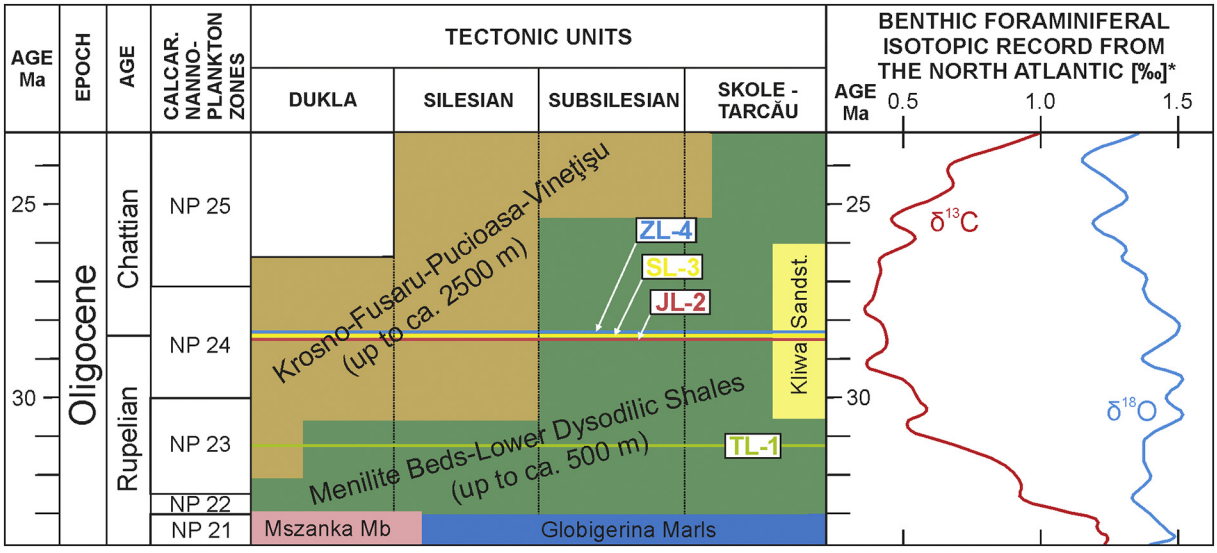

Fig. 2. General stratigraphic relationships and positions of the coccolith limestone horizons (based on: Martini, 1971; Haczewski, 1989; Rögl, 1998; Bąk, 1999; Melinte, 2005; Kotlarczyk et al., 2006; Ciurej, 2009). Calcareous nannoplankton zones after Martini (1971); TL-1 – Tylawa, JL-2 – Jasło, SL-3 – Sokoliska and ZL-4 – Zagórz limestone horizons. JL-2, SL-3 and ZL-4 were laid down during a few tens of thousands years. The numerical age based on the GTS 2012 (Gradstein et al., 2012). The benthic foraminiferal isotopic curves redrawn from Cramer et al. (2009).

of the following statistical properties determined for each sample: no. of measurements, median value, standard deviation, maximum value, contents framboids with diameters > 10 μm (Table 1).

Content, distribution and preservation of calcareous nannoplankton were studied in 46 limestone samples. Observations were performed on 21 smear slides (see Perch-Nielsen, 1985) and 52 thin sections. All thin sections were examined using SEM in the Charge Contrast Imaging mode (see Ciurej, 2010). Smear slides, prepared from the same specimens used for thin sections, were examined under the polarizing microscope at a 100× magnification in plane and cross polarized light. Taxonomic identification was carried out on the basis of both methods and the literature. Standard palynological preparation was applied to 68 samples. Taxonomy follows those cited in Fensome and Williams (2004), unless stated otherwise. We interpret paleoenvironmental conditions from dinocyst assemblages based on Sluijs et al. (2005) and Pross and Schmiedl (2002). Foraminifers were found in 13 out of 90 thin sections. Most of the samples (11) represent JL-2. Every thin section was divided into 3 to 15 subsamples and examined under a NIKON SMZ-1500 stereomicroscope with normal transmitted light.

3.2. Organic geochemical analyses

Total organic carbon (TOC) and total sulfur (TS) contents together with lipid biomarkers were analyzed in sixteen samples (15 limestones, 1 mudstone) from all limestone horizons. The samples were collected from nine sections in the Silesian, Subsilesian and Skole-Tarcău units (Table 1). Samples were grinded and analyzed for apolar lipid biomarkers following Sinninghe Damsté et al. (2014; see Appendix for details). Briefly, they were extracted with a DIONEX Accelerated Solvent Extractor (ASE 200) and the extract was separated into apolar, aromatic and polar fractions via alumina pipette column chromatography. Compounds were analyzed on an Agilent Gas Chromatograph. Compounds were detected by flame ionization detection. Molecular identification of the compounds was performed on an Agilent 7890B gas chromatograph coupled to an Agilent 5977A mass spectrometer. TOC and TS contents were analyzed using a Leco SC-632 instrument.

3.3. Isotopic measurements

$\delta^{13}C_{org}$ and $\delta^{15}N_{org}$ were measured in 41 samples (32 limestones, 9 mudstones) with an elemental analyzer coupled to an isotope ratio mass spectrometer (IRMS). However, N isotope measurements were unsuccessful for 18 limestone samples due to insufficient N contents. Analytical error of the measurements was better than ± 0.3‰ for $\delta^{13}C_{org}$ and ± 0.2‰ for $\delta^{15}N_{org}$. $\delta^{13}C_{org}$ and $\delta^{15}N_{org}$ are reported relative to V-PDB and atmospheric nitrogen, respectively.

177 stable C and O isotope measurements in carbonates were performed using a Thermo KIEL IV Carbonate Device connected on-line to an IRMS in a Dual Inlet system. The reproducibility of the measurements (1σ) was ± 0.03‰ for $\delta^{13}C$ and ± 0.07‰ for $\delta^{18}O$. $\delta^{13}C$ and $\delta^{18}O$ are reported relative to V-PDB. Powders for stable C and O isotope analyses were taken by using sintered diamond microdrills on vertical or oblique planes. Multiple subsamples were taken from some specimens along vertical transects. Material obtained by this technique was usually collected from a set of several adjacent laminae. However, some specimens contained unusually thick laminae and material could be collected from individual laminae with a scalpel or a MicroMill microsampling device equipped with tungsten drill bits (~0.2 mm in diameter).

S isotope measurements were conducted in 35 samples (33 limestones, 2 mudstones), which contained framboidal pyrites as the dominant sulfide with very rare euhedral grains. Pyritic S was extracted and precipitated as Ag_2S by the chromium reduction method (Canfield et al., 1986; Goldberg et al., 2005). Ag_2S precipitates were combusted at 1020 °C using a Thermo Flash Elemental Analyzer 1112HT. $^{34}S/^{32}S$ measurements of the released SO_2 gas were carried out with a Thermo Delta V Advantage IRMS in a continuous flow system following the procedure of Grassineau et al. (2001). Results are reported as the $\delta^{34}S$ notation against the V-CDT standard with reproducibility (1σ) better than ± 0.2‰.

Sr isotope measurements were conducted in 10 limestone samples (~50 mg each) with a Finnigan MAT 261 mass spectrometer. Powdered samples were dissolved on a hot plate (~100 °C) using 0.75 N hydrochloric acid. Sr separation followed the miniaturized chromatographic

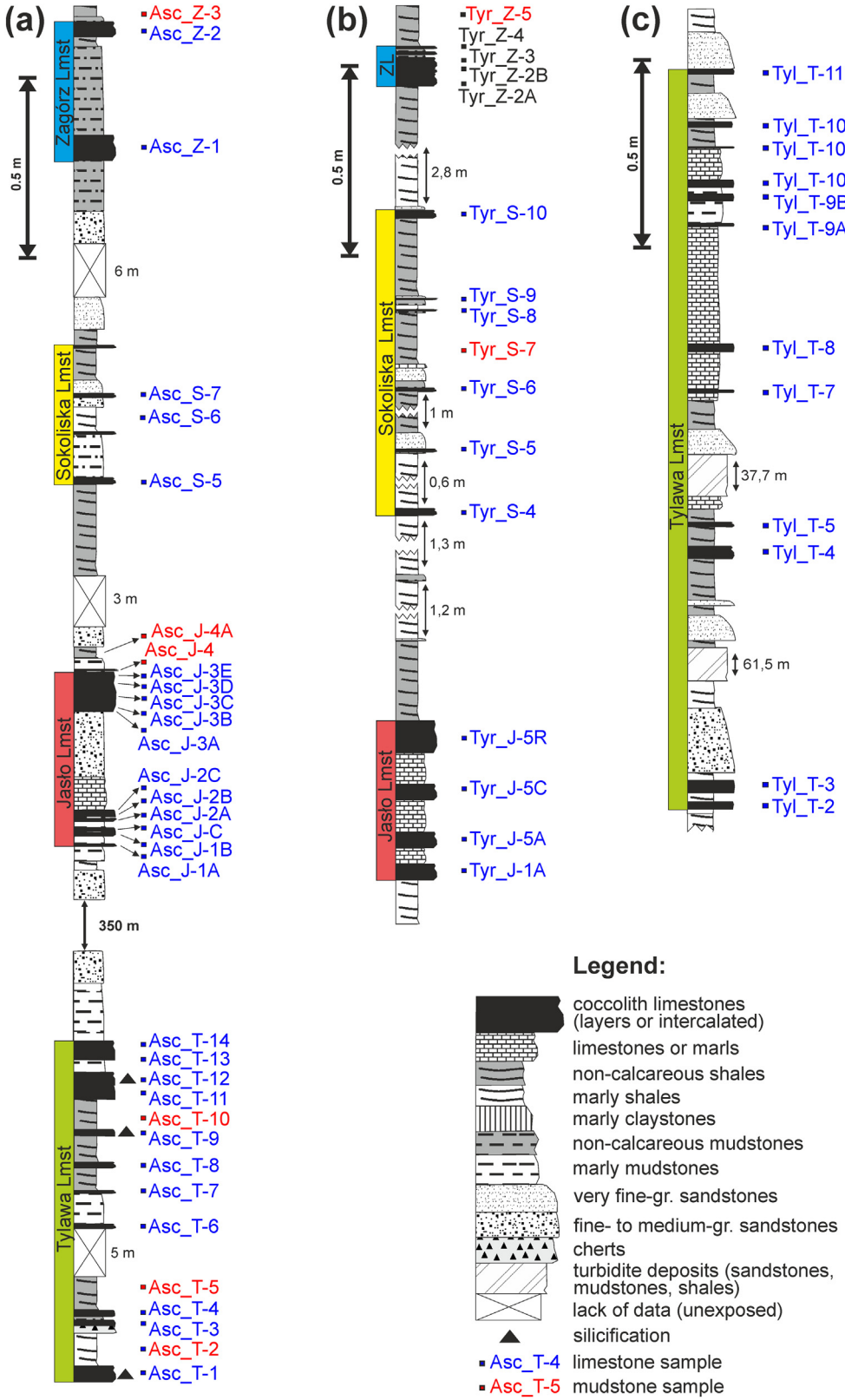

Fig. 3. Selected lithologs showing the distribution of all coccolith limestones horizons and positions of samples collected for sections in Ascuns (a), Tyrawa Solna (b) and Tylawa (c).

Table 1
Results of isotopic analyses ($\delta^{13}C$, $\delta^{18}O$ and $^{87}Sr/^{86}Sr$ in carbonates, $\delta^{13}C$ in total organic matter, $\delta^{34}S$ in pyrite), measurements of framboidal pyrite diameters and presence of 28,30-dinorhopane biomarker.

T Y L A W A L M S T (T L - 1)												
Section	Unit	Sample	Material type	$\delta^{13}C_{carb}$	$\delta^{18}O_{carb}$	Paleotemp.	$^{87}Sr/^{86}Sr$	Error [$\times 10^6$]	^{87}Sr enrichm. [$\times 10^6$]	$\delta^{13}C_{org}$	$\delta^{15}N_{org}$	$\delta^{34}S$
				[‰]	[‰]	[°C]				[‰]	[‰]	[‰]
Ascuns	Skole-Tarcău	Asc_T-1	Several laminae	−2.0	−4.2	39.7	0.708181	± 11	210	−27.6		−23.7
		Asc_T-1A	Light lamina	−1.9	−4.3	40.5						
		Asc_T-1B	Light lamina	−2.2	−4.8	43.1						
		Asc_T-1C	Light lamina	−1.9	−4.6	42.1						
		Asc_T-2	Mudstone							−27.7		
		Asc_T-3B	Light lamina	−1.3	−3.9	38.2						
		Asc_T-3C	Light lamina	−1.2	−3.7	36.9						
		Asc_T-3D	Light lamina	−1.7	−3.8	37.6						
		Asc_T-4A	Light lamina	−1.4	−4.0	38.5						
		Asc_T-4B	Light lamina	−1.2	−3.9	37.9						
		Asc_T-5	Mudstone									
		Asc_T-9	Several laminae	−2.3	−4.3	40.1				−28.7		−21.6
		Asc_T-10	Mudstone							−27.2	0.6	
Bezmiechowa Górna	Subsilesian	Bez_T-3A	Several laminae	−1.6	−2.2	29.3						
		Bez_T-3B	Several laminae	−1.7	−2.8	32.1						
		Bez_T-5A	Several laminae	−1.5	−2.1	28.9				−29.5	−4.1	
		Bez_T-5D	Several laminae	−2.1	−2.8	32.1						
		Bez_T-6	Mudstone							−26.9	0.3	
Fântânele	Transilvanian Basin	Fan_T-1	Several laminae							−27.4		
		Fan_T-2A	Light lamina	−1.8	−2.4	30.2	0.708085	± 8	117			−19.9
		Fan_T-2B	Light lamina	−1.9	−2.5	30.8						
		Fan_T-2C	Dark lamina	−2.2	−2.7	31.6						
		Fan_T-2D	Dark lamina	−2.4	−2.6	31.4						
Wisłok Wielki	Dukla	Wis_T-1A	Several laminae	−0.7	−5.8	48.9						
		Wis_T-1B	Several laminae	0.9	−4.2	39.7						
		Wis_T-1C	Several laminae	0.2	−5.2	45.6						
		Wis_T-1D	Several laminae	−0.1	−5.3	46.0						
Rudawka Rymanowska	Silesian	Rud_T-1A	Light lamina	−0.6	−4.3	40.4						
		Rud_T-1B	Several laminae							−24.2	−1.3	
		Rud_T-1	Light lamina	−0.4	−4.8	43.3						
		Rud_T-9A	Light lamina	−1.4	−4.4	40.9						
		Rud_T-9B	Light lamina	−1.1	−4.5	41.7						
		Rud_T-6A	Several laminae							−26.1	−1.1	
		Rud_T-6A1	Light lamina	−0.7	−4.3	40.3						−28.7
		Rud_T-6A2	Light lamina	−0.5	−4.2	40.0						
		Rud_T-6A3	Light lamina	−0.5	−4.1	39.3						
		Rud_T-6D1	Light lamina	−1.2	−4.1	39.5						
		Rud_T-6D2	Light lamina	−0.9	−4.9	43.5						
		Rud_T-6D3	Light lamina	−1.3	−3.7	36.9						
		Rud_T-4	Light lamina	−0.3	−4.8	43.4						
		Rud_T-3	Light lamina	−0.1	−4.4	41.0						
		Rud_T-2A	Light lamina	−0.1	−4.7	42.3						
		Rud_T-2B	Light lamina	−0.1	−4.7	42.5						
		Rud_T-2C	Light lamina	−0.2	−4.6	41.7						
		Rud_T-11A1	Light lamina	−1.6	−5.0	44.4						
		Rud_T-11A2	Light lamina	−2.0	−5.1	44.6						
		Rud_T-11B	Light lamina	−1.6	−4.7	42.6	0.708218	± 12	246			−31.4
Suslăneşti	Skole-Tarcău	Sus_T-2	Several laminae							−27.3		
		Sus_T-7A	Several laminae	−1.6	−2.6	31.5				−28.0		−18.5

(*continued on next page*)

Table 1 (*continued*)

T Y L A W A L M S T (T L - 1)

Section	Unit	Sample	Material type	$\delta^{13}C_{carb}$	$\delta^{18}O_{carb}$	Paleotemp.	$^{87}Sr/^{86}Sr$	Error [$\times 10^6$]	^{87}Sr enrichm. [$\times 10^6$]	$\delta^{13}C_{org}$	$\delta^{15}N_{org}$	$\delta^{34}S$
				[‰]	[‰]	[°C]				[‰]	[‰]	[‰]
Tylawa	Dukla	Tyl_T-2	Several laminae	−0.3	−6.2	50.9						
		Tyl_T-3	Several laminae	−0.5	−5.9	49.2	0.708242	± 10	272	−26.2	−2.8	−29.7
		Tyl_T-5	Light lamina	0.0	−4.9	43.9						
		Tyl_T-8	Light lamina	0.9	−5.3	45.7						
		Tyl_T-9B1	Light lamina	0.7	−5.3	46.1						−29.7
		Tyl_T-9B2	Light lamina	0.6	−5.7	48.1						
		Tyl_T-10A	Light lamina	0.9	−4.7	42.7						
		Tyl_T-10B	Light lamina	1.3	−4.3	40.6						
		Tyl_T-10C	Light lamina	0.6	−5.0	44.2						
		Tyl_T-11	Light lamina	0.4	−4.9	43.8						
Wujskie	Subsilesian	Wuj_T-1	Mudstone									
		Wuj_T-7G	Several laminae	−2.0	−2.4	30.5						−2.1
		Wuj_T-9	Mudstone									
		Wuj_T-14B	Several laminae	−1.3	−2.9	33.0				−26.1	−1.4	−30.2
			Mean[a]	−0.9	−4.2	40.0				−27.1	−2.1	−23.5
			sd	1.0	1.0	5.5				1.5	1.3	8.9

T Y L A W A L M S T (T L - 1)

Section	Framboidal pyrite diameters					TOC	TS	28,30-Dinorhopane	*Dinoflagellata* assemblages[b]		
	Median [μm]	SD [μm]	Max. [μm]	> 10 μm [%]	*n*	[%]	[%]		*n*	Stratification-related sp. [%]	Productivity-related sp. [%]
Ascuns	4.3	1.4	8.5	0.0	1836				Barren		
									Barren		
									Barren		
									Barren		
						1.0	0.1	Not detected			
Bezmiechowa Górna											
						4.0	0.9	Not detected			
Fântânele									Barren		
	3.3	1.3	10.6	0.1	1271				Barren		
Wisłok Wielki											

(*continued on next page*)

Table 1 (*continued*)

T Y L A W A L M S T (T L - 1)											
Section	Framboidal pyrite diameters					TOC	TS	28,30-Dinorhopane	*Dinoflagellata* assemblages[b]		
	Median [μm]	SD [μm]	Max. [μm]	> 10 μm [%]	*n*	[%]	[%]		*n*	Stratification-related sp. [%]	Productivity-related sp. [%]
Rudawka Rymanowska									Barren		
						0.5	0.7	Not detected	3	0	67
						3.5	0.8	Not detected			
	3.8	1.3	17.2	0.2	3037						
Susłaneşti						1.5	0.7	Not detected			
Tylawa											
	5.0	1.2	15.8	0.1	2673				Barren		
									Barren		
Wujskie									1	0	0
									Barren		
									barren		
						2.8	1.1	Not detected	barren		
	4.1			0.1		2.2	0.7				
	0.7			0.1		1.4	0.3				

(*continued on next page*)

Table 1 (*continued*)

J A S Ł O L M S T (JL - 2)

Section	Unit	Sample	Material type	$\delta^{13}C_{carb}$	$\delta^{18}O_{carb}$	Paleotemp.	$^{87}Sr/^{86}Sr$	Error [$\times 10^6$]	^{87}Sr enrichm. [$\times 10^6$]	$\delta^{13}C_{org}$	$\delta^{15}N_{org}$	$\delta^{34}S$
				[‰]	[‰]	[°C]				[‰]	[‰]	[‰]
Ascuns	Skole-Tarcău	Asc_J-1A	Several laminae, dolom.	0.2	−5.3					−25.6		−28.5
		Asc_J-3A	Several laminae							−23.7		
		Asc_J-3B	Several laminae	1.3	−6.1	50.7				−24.6		−31.3
		Asc_J-3D1	Light lamina	2.1	−6.5	53.0						
		Asc_J-3D2	Light lamina	2.1	−6.4	52.5						
		Asc_J-3D3	Light lamina	2.2	−6.4	52.5						
		Asc_J-3E	Several laminae	1.5	−4.5	41.7				−23.9	0.2	−33.7
		Asc_J-4	Mudstone	1.9	−1.8					−24.7	1.2	−36.6
		Asc_J-4A	Mudstone									
Buciumeni	Skole-Tarcău	Buc_J-1	Several laminae									
		Buc_J-2	Mudstone									
		Buc_J-6	Several laminae	1.9	−2.2	29.2						−34.5
		Buc_J-6A	Several laminae, dolom.							−24.6		−30.0
Bukowiec nad Solinką	Silesian	Buk_J-8A										
		Buk_J-8B1	Light lamina	2.1	−5.3	45.8						
		Buk_J-8B2	Light lamina	2.3	−5.0	44.1						
		Buk_J-8B3	Mostly light lamina	2.3	−5.4	46.6						
		Buk_J-8B4	Mostly light lamina	1.6	−5.8	48.5						
		Buk_J-8B5	Mostly light lamina	2.3	−5.3	45.8						−30.3
		Buk_J-8B6	Mostly light lamina	2.0	−5.0	44.1						
Dobra	Skole	Dob_J-6A	Light lamina	−1.8	−4.2	39.9						
		Dob_J-6B	Light lamina	−1.4	−4.1	39.4						
		Dob_J-6C	Light lamina	−1.0	−4.3	40.4						
Wisłok Wielki	Dukla	Wis_J-3A	Light lamina	−0.3	−2.0	28.4						
		Wis_J-3B	Light lamina	−0.1	−2.0	28.4						
		Wis_J-4C	Light lamina	1.0	−2.5	30.8						
Halicz	Silesian	Hal_J-2B	Several laminae							−24.0	0.3	
		Hal_J-3B	Mostly light lamina	2.5	−4.4	40.8						
		Hal_J-3C	Mostly light lamina	2.8	−4.2	39.7						
		Hal_J-4A	Mostly light lamina	2.4	−4.8	43.2						
		Hal_J-4B	Mostly light lamina	2.7	−4.5	41.3						
		Hal_J-5	Several laminae	2.0	−5.0	44.0						−34.6
Krępak	Skole	Kre_J-5	Several laminae	−2.7	−4.0	38.6						−28.5
		Kre_J-5A	Light lamina	−2.3	−4.0	38.6						
		Kre_J-5B	Light lamina	−2.3	−3.9	38.4						
		Kre_J-5C	Light lamina	−2.7	−3.9	38.3						

(*continued on next page*)

Table 1 (*continued*)

JASŁOLMST (JL - 2)

Section	Unit	Sample	Material type	$\delta^{13}C_{carb}$ [‰]	$\delta^{18}O_{carb}$ [‰]	Paleotemp. [°C]	$^{87}Sr/^{86}Sr$	Error [$\times 10^6$]	^{87}Sr enrichm. [$\times 10^6$]	$\delta^{13}C_{org}$ [‰]	$\delta^{15}N_{org}$ [‰]	$\delta^{34}S$ [‰]
Olchowski Potok	Silesian	Olc_J-0	Several laminae									
		Olc_J-1A	Light lamina	1.6	−4.0	38.8						
		Olc_J-1B	Light lamina	1.7	−4.0	38.5	0.708437	± 10	368			−36.2
		Olc_J-1C	Light lamina	2.4	−4.0	38.9						
		Olc_J-1E	Light lamina	1.9	−4.2	40.0						
		Olc_J-1F	Light lamina	2.2	−4.3	40.5						
		Olc_J-1G	Light lamina	1.3	−3.9	37.9						
		Olc_J-1H	Light lamina	0.6	−3.4	35.5						
		Olc_J-2	Several laminae							−23.7	0.3	
		Olc_J-2H	Light lamina	1.6	−3.8	37.4						
		Olc_J-2D	Light lamina	1.4	−4.3	40.1						
		Olc_J-2I	Light lamina	1.8	−3.6	36.8						
		Olc_J-3C	Light lamina	2.0	−3.7	37.0						
Paltinu	Skole-Tarcău	Pal_J-4A	Non-laminated	2.2	−5.6	47.6				−26.4		−44.0
		Pal_J-5	Several laminae	1.6	−6.1	50.3	0.708332	± 10	263	−25.4		−29.5
		Pal_J-7A	Several laminae	2.2	−6.7	54.0				−23.5	0.3	−31.7
		Pal_J-7AB	Several laminae	2.4	−6.5	53.0				−24.6		−35.9
		Pal_J-7B	Several laminae	2.2	−6.4	52.0						−34.7
		Pal_J-7B1	Light lamina	2.6	−6.7	54.2						
		Pal_J-7B2	Light lamina	2.5	−6.4	52.3						
		Pal_J-7B3	Light lamina	2.5	−6.6	53.7						
		Pal_J-7C	Mudstone	1.1	−2.9					−24.9		−37.4
Przysietnica	Subsilesian	Prz_J-1	Several laminae	0.9	−3.3	35.0				−24.7		−31.8
Sękowa	Silesian	Sek_J-1	Light lamina	2.2	−3.7	37.0						
		Sek_J-2	Light lamina	2.1	−4.3	40.4						−24.0
		Sek_J-3B	Light lamina	0.7	−4.3	40.3						
		Sek_J-4	Light lamina	1.9	−4.2	39.9						
		Sek_J-5	Light lamina	2.4	−4.0	38.6						
		Sek_J-6	Light lamina	2.2	−3.7	37.3						
Serednica	Skole	Ser_J-6A	Light lamina	1.5	−5.0	44.3						
		Ser_J-6B	Light lamina	1.9	−5.1	44.7						
		Ser_J-6C	Mostly light lamina	1.7	−5.2	45.2						−36.9
		Ser_J-6D	Mostly light lamina	1.7	−4.8	43.1						
		Ser_J-6E	Mostly dark lamina	1.1	−5.0	44.1						
		Ser_J-6F	Mostly light lamina	1.6	−5.1	44.7						
		Ser_J-6G	Mostly dark lamina	1.2	−5.2	45.2						
Terka	Silesian	Ter_J-8A	Light lamina	1.9	−4.6	42.2						
		Ter_J-8C	Light lamina	2.2	−4.5	41.5						
Tyrawa Solna	Skole	Tyr_J-0	Mudstone							−24.2	0.3	
		Tyr_J-1A	Light lamina	1.4	−4.7	42.6	0.708331	± 15	257	−23.4		−32.0

(*continued on next page*)

Table 1 (*continued*)

JASŁO LMST (JL - 2)

Section	Unit	Sample	Material type	$\delta^{13}C_{carb}$	$\delta^{18}O_{carb}$	Paleotemp.	$^{87}Sr/^{86}Sr$	Error [$\times 10^6$]	^{87}Sr enrichm. [$\times 10^6$]	$\delta^{13}C_{org}$	$\delta^{15}N_{org}$	$\delta^{34}S$
				[‰]	[‰]	[°C]				[‰]	[‰]	[‰]
Tyskowa	Silesian	Tys_J-9A	Light lamina	1.7	−5.4	46.5						
		Tys_J-9C	Light lamina	2.0	−4.9	43.7						
			Mean[a]	1.4	−4.7	42.5				−24.5	0.2	−32.7
			sd	1.4	1.1	6.2				0.9	0.1	4.3

JASŁO LMST (JL - 2)

Section	Framboidal pyrite diameters					TOC	TS	28,30-Dinorhopane	*Dinoflagellata* assemblages[b]		
	Median [μm]	SD [μm]	Max. [μm]	> 10 μm [%]	*n*	[%]	[%]		*n*	Stratification-related sp. [%]	Productivity-related sp. [%]
Ascuns	4.0	2.2	27.5	2.1	982						
						0.3	0.2	Common			
	4.2	1.5	8.6	0.0	357				Barren		
	3.6	1.3	10.1	0.0	2271	3.7	2.7	Common			
						7.3	4.1	Common	1	0	100
									Barren		
Buciumeni									1	0	100
									41	24	54
	3.7	1.3	11.2	0.2	943						
	4.1	1.6	15.2	0.6	175	0.8	0.5	Not detected	37	11	27
Bukowiec nad Solinką									7	0	0
									33	6	12
	4.3	1.4	7.0	0.0	97						
Dobra											
Wisłok Wielki											
Halicz											
Krępak	4.4	1.6	24.4	0.7	910				12	0	8

(*continued on next page*)

Table 1 (*continued*)

J A S Ł O L M S T (J L - 2)											
Section	Framboidal pyrite diameters					TOC	TS	28,30-Dinorhopane	*Dinoflagellata* assemblages[b]		
	Median [μm]	SD [μm]	Max. [μm]	> 10 μm [%]	*n*	[%]	[%]		*n*	Stratification-related sp. [%]	Productivity-related sp. [%]
Olchowski Potok									8	25	38
	4.1	1.6	9.8	0.0	498						
									91	9	24
Paltinu	7.5	3.1	32.4	15.2	985						
	4.7	2.0	12.4	2.4	210						
	4.5	1.5	8.9	0.0	103				32	0	9
	3.7	1.3	9.1	0.0	518				2	0	0
									6	0	50
Przysietnica Sękowa	4.3	1.2	8.6	0.0	70	0.1	0.2	Not detected	Barren		
Serednica	3.9	1.4	8.2	0.0	404				68	0	7
									53	2	62
Terka											
Tyrawa Solna											
	4.4	1.6	10.8	0.2	535	0.7	0.2	Abundant	2	0	50
Tyskowa											
	4.4			1.4		1.1	0.8				
	0.9			3.9		1.4	1.1				

(continued on next page)

SOKOLISKALMST (SL - 3)

Section	Unit	Sample	Material type	$\delta^{13}C_{carb}$	$\delta^{18}O_{carb}$	Paleotemp.	$^{87}Sr/^{86}Sr$	Error [$\times 10^6$]	^{87}Sr enrichm. [$\times 10^6$]	$\delta^{13}C_{org}$	$\delta^{15}N_{org}$	$\delta^{34}S$
				[‰]	[‰]	[°C]				[‰]	[‰]	[‰]
Ascuns	Skole-Tarcău	Asc_S-5A	Dark lamina	0.1	−4.3	40.1						
		Asc_S-5B	Several laminae	0.5	−4.8	43.0						
		Asc_S-5C	Several laminae	0.3	−5.5	46.8						
		Asc_S-6	Several laminae									
Bukowiec nad Solinką	Silesian	Buk_S-1	Several laminae	1.2	−4.7	42.6				−24.6	0.3	
		Buk_S-2	Dark lamina	1.8	−4.6	42.2						
		Buk_S-3	Several laminae	1.8	−4.4	40.9						
		Buk_S-3A	Mudstone									
		Buk_S-4	Several laminae	1.9	−4.9	43.9						
		Buk_S-5	Several laminae	1.8	−4.1	39.5						
		Buk_S-6	Several laminae	1.4	−4.7	42.5				−25.4		
		Buk_S-7	Several laminae	1.8	−4.5	41.5	0.708510	± 10	441	−24.8	0.3	
		Buk_S-7A	Mudstone									
Halicz	Silesian	Hal_S-2A	Mudstone									
		Hal_S-3	Several laminae									
		Hal_S-6	Several laminae									
Tyrawa Solna	Skole	Tyr_S-4	Several laminae	1.1	−3.5	36.0				−24.4	0.3	−35.0
		Tyr_S-6A	Light lamina	1.3	−4.0	38.7						
		Tyr_S-6B	Light lamina	1.5	−3.8	37.5						
		Tyr_S-6C	Light lamina	1.6	−3.8	37.7						
		Tyr_S-7	Mudstone							−24.4	−0.6	
		Tyr_S-10A	Light lamina	0.9	−4.0	38.8						
		Tyr_S-10B	Light Lamina	1.0	−3.8	37.8						
			Mean[a]	1.3	−4.3	40.6				−24.8	0.3	
			sd	0.6	0.5	2.8				0.2	0.0433	

SOKOLISKALMST (SL - 3)

Section	Framboidal pyrite diameters					TOC	TS	28,30-Dinorhopane	*Dinoflagellata* assemblages[b]		
	Median [μm]	SD [μm]	Max. [μm]	> 10 μm [%]	*n*	[%]	[%]		*n*	Stratification-related sp. [%]	Productivity-related sp. [%]
Ascuns											
	3.9	1.7	26.7	0.7	5313				Barren		
									Barren		
Bukowiec nad Solinką									19	0	5
									5 barren	0	0
									3	0	0
									2	0	0
Halicz									20	20	10
									36	0	14
									14	0	14

(*continued on next page*)

Table 1 (*continued*)

SOKOLISKA LMST (SL - 3)

Section	Framboidal pyrite diameters					TOC	TS	28,30-Dinorhopane	*Dinoflagellata* assemblages[b]		
	Median [μm]	SD [μm]	Max. [μm]	> 10 μm [%]	*n*	[%]	[%]		*n*	Stratification-related sp. [%]	Productivity-related sp. [%]
Tyrawa Solna	4.8	1.8	27.6	0.4	725	1.3	1.3	Abundant	2	0	50
									barren		
	4.3			0.6							
	0.6			0.2							

ZAGÓRZ LMST (ZL - 4)

Section	Unit	Sample	Material type	$\delta^{13}C_{carb}$	$\delta^{18}O_{carb}$	Paleotemp.	$^{87}Sr/^{86}Sr$	Error [$\times 10^6$]	^{87}Sr enrichm. [$\times 10^6$]	$\delta^{13}C_{org}$	$\delta^{15}N_{org}$	$\delta^{34}S$
				[‰]	[‰]	[°C]				[‰]	[‰]	[‰]
Ascuns	Skole-Tarcău	Asc_Z-1A	Light band	0.2	−5.8	48.9				−24.6	2.2	−28.7
		Asc_Z-1B	Light band	0.0	−5.8	48.8						
		Asc_Z-1C	Light band	0.1	−5.9	49.2						
		Asc_Z-1D	Light band	−0.1	−6.0	49.9						
		Asc_Z-1E	Light band	0.0	−6.0	49.7						
		Asc_Z-1F	Light band	0.0	−5.8	48.5						
		Asc_Z-3	Mudstone							−25.2	2.0	
Czereszenka	Silesian	Cze_Z-1	Light band	1.1	−4.0	38.7						
		Cze_Z-2	Light band	1.0	−4.2	39.9						
		Cze_Z-6	Light band	0.9	−4.3	40.2						
		Cze_Z-7A	Light band	1.1	−4.2	39.7						
		Cze_Z-7B	Mostly dark lamina	1.0	−4.1	39.5						
		Cze_Z-8A	Light band	1.5	−3.7	37.3				−25.3	0.3	
		Cze_Z-8B	Dark lamina	1.6	−3.7	37.2						−20.9
		Cze_Z-8C	Light band	1.7	−3.7	37.0						
		Cze_Z-8D	Dark band	1.8	−3.7	37.2						
		Cze_Z-8E	Light band	1.6	−3.8	37.7						
		Cze_Z-9	Light band	2.1	−3.0	33.1						
		Cze_Z-11	Light band	1.4	−4.3	40.5						
		Cze_Z-18	Light band	1.7	−4.9	43.9						
		Cze_Z-20	Light band	1.4	−4.8	43.0						
		Cze_Z-22	Mostly dark lamina	1.8	−4.6	42.0						
		Cze_Z-23	Light band	1.8	−4.6	41.9						
Dydiowa	Silesian	Dyd_Z-0A	Mudstone									
		Dyd_Z-5A	Light band	1.1	−4.2	39.9				−25.2		
		Dyd_Z-5B	Dark lamina	0.9	−4.2	39.6						
		Dyd_Z-7A	Light band	1.4	−4.1	39.2	0.708503	± 9	435	−25.1	−2.5	6.4
		Dyd_Z-7B	Dark lamina	1.7	−3.8	37.5						
		Dyd_Z-7C	Light band	1.6	−3.7	37.4						
		Dyd_Z-7D	Dark band	1.6	−3.4	35.7						
		Dyd_Z-7E	Light band	1.6	−3.9	38.3						
		Dyd_Z-11	Light band	1.6	−4.2	39.7						

(continued on next page)

Table 1 (*continued*)

Z A G Ó R Z L M S T (Z L - 4)												
Section	Unit	Sample	Material type	$\delta^{13}C_{carb}$	$\delta^{18}O_{carb}$	Paleotemp.	$^{87}Sr/^{86}Sr$	Error [$\times 10^6$]	^{87}Sr enrichm. [$\times 10^6$]	$\delta^{13}C_{org}$	$\delta^{15}N_{org}$	$\delta^{34}S$
				[‰]	[‰]	[°C]				[‰]	[‰]	[‰]
Tyrawa Solna	Skole	Tyr_Z-2A1	Light band	0.0	−4.3	40.3				−24.5	0.8	
		Tyr_Z-2A2	Light band	0.0	−4.3	40.5						
			Tyr_Z-2A3	Light band	0.0	−4.3	40.5					
		Tyr_Z-2B1	Light band	0.1	−4.6	42.1	0.708405	± 9	337			−30.4
		Tyr_Z-2B2	Light band	0.0	−4.7	42.5						
		Tyr_Z-2B3	Light band	0.0	−4.6	41.8						
		Tyr_Z-3A	Light band	0.0	−3.8	37.5						
		Tyr_Z-3B	Light band	0.2	−3.8	37.7						
		Tyr_Z-3C	Light band	0.5	−3.5	35.8						
		Tyr_Z-4	Dark lamina	1.1	−4.8	42.8						
Tyr_Z-5	Mudstone							−24.9	0.3			
			Mean[a]	0.9	−4.4	40.8				−24.9	0.2	−18.4
			sd	0.7	0.8	4.2				0.4	2.0	17.0

Z A G Ó R Z L M S T (Z L - 4)											
Section	Framboidal pyrite diameters					TOC	TS	28,30-Dinorhopane	*Dinoflagellata* assemblages[b]		
	Median [μm]	SD [μm]	Max. [μm]	> 10 μm [%]	*n*	[%]	[%]		*n*	Stratification-related sp. [%]	Productivity-related sp. [%]
Ascuns	4.1	1.1	7.5	0.0	166	0.1	0.1	Common	29	69	7
Czereszenka									14	29	21
									195	0	7
									12	25	33
									92	0	8
Dydiowa									2	50	0
	3.3	1.5	7.4	0.0	29	0.5	0.0	Not detected	51	0	10
Tyrawa Solna									16	13	13

(*continued on next page*)

Table 1 (*continued*)

Section	Framboidal pyrite diameters					TOC	TS	28,30-Dinorhopane	*Dinoflagellata* assemblages[b]		
	Median [μm]	SD [μm]	Max. [μm]	> 10 μm [%]	*n*	[%]	[%]		*n*	Stratification-related sp. [%]	Productivity-related sp. [%]
ZAGÓRZ L M S T (ZL - 4)											
	4.9	2.6	15.1	3.8	340	1.0	0.2	abundant			
									1	100	0
	4.1			1.3		0.5	0.1				
	0.8			2.2		0.5	0.1				

[a] $\delta^{13}C_{carb}$, $\delta^{18}O_{carb}$ and paleotemperature mean values are calculated only for limestone samples without dolomitisation; $\delta^{34}S$, $\delta^{13}C_{org}$, TOC and TS mean values are calculated only for limestone samples.

[b] Contents of stratification-related species (*Homotryblium* spp.) and productivity-related species (*Selenopemphix nephroides*, *Deflandrea phosphoritica*, *Brigantedinium* sp.) are given as relative abundances.

technique described by Pin et al. (1994) with modifications introduced by Dopieralska (2003). All the measured $^{87}Sr/^{86}Sr$ values were adjusted to the preferred value of 0.710248 for NIST-987. The analytical error of the measurements was up to ± 1.2×10^{-5} (Table 1).

4. Results

4.1. Composition of the limestones and preservation of calcareous nannoplankton

The limestones are white, yellow or light grey and usually finely laminated (Fig. 4). They are intercalated with siliciclastic sediments, mostly fine-grained turbidites or organic C-rich shales (Fig. 2). The limestones exhibit characteristic lamination that represents seasonal variability and may serve as the basis for correlation of some laminae sets (Fig. 4). Similar lamination patterns are identified in sections located even > 500 km apart (Haczewski, 1989, 1996). The composition and fabric of the limestones is similar in all horizons. Some differences exist between them, but the structure of each horizon is laterally persistent. The limestones predominantly consist of alternating dark (brown to black) and light (light grey or yellow) up to 600 μm thick laminae (Fig. 4). The dark laminae are thinner, mostly < 100 μm. The light laminae exhibit micronodular fabric and consist mainly of lensoidal fecal pellets of zooplankton, probably copepods (cf. Roth et al., 1975; Honjo and Roman, 1978), and irregular aggregates that may represent marine snow (see discussion in Haczewski, 1989 and in Ciurej, 2009). The pellets in the light laminae are almost entirely composed of coccolithophore skeletal remains. Apart from these typical fine laminae, rare light laminae with distinctively different composition and texture appear as well. They have greater and variable thickness (from 0.5 to 12 mm), exhibit homogeneous texture and were most likely formed by redeposition of limy sediments that represent allochtonous material composed of either older or synchronous sediments from shallower areas (Haczewski, 1996). These laminae were avoided in this work.

Preservation of calcareous nannoplankton is excellent or good in TL-1, JL-2 and SL-3, whilst it is good or moderate in ZL-4. Even delicate morphological details of coccoliths are well-preserved in the light laminae, such as the central area structures that are clearly visible under SEM, proximal shields are not detached from the distal ones (Fig. 4A-2). Traces of dissolution, secondary overgrowth or mechanical fragmentation are present only locally, mainly in ZL-4. Complete, intact coccospheres are often found in the light laminae; some laminae are composed exclusively of coccospheres clustered in the pellets (Fig. 4A-2). The coccolithophores represent low-diversity assemblages dominated by the endemic *Reticulofenestra ornata* Müller (~90% of all specimens) in TL-1 and by *Cyclicargolithus floridanus* (Roth et Hay) Bukry (80–85% of all specimens) in JL-2, SL-3 and ZL-4 (Ciurej, 2009). The matrix present between the pellets in the light laminae is scarce and mostly composed of clay minerals, quartz, micas, feldspars, carbonate grains, pyrite and organic matter. The limestones contain various amounts of carbonate and silica cements. Carbonate cements are mostly represented by microspar anhedral calcite and disseminated rhombohedral dolomite. Many light laminae have little or no cement (Fig. 4A-2). Others contain cements that tightly fill the coccospheres and spaces between loose coccoliths (Fig. 3B-2 and C-2). Only two samples of JL-2 from Romania (Ascuns and Buciumeni sections) are partly dolomitized. Silica cement is much less abundant and limited to individual pellets. Detrital material and organic matter are much more abundant in the dark laminae (Fig. 4A-3–D-3), whilst silica and carbonate cements (sub- to euhedral rhombohedral dolomite) occur only occasionally (Fig. 4A-3). Phosphatic fish fragments are sometimes accumulated along some dark laminae.

Fabric of ZL-4 is quite different than that of the other limestone horizons. ZL-4 is composed of parallel but undulating, diffuse bands that only slightly differ in shades of grey color (Fig. 4D-1). Individual

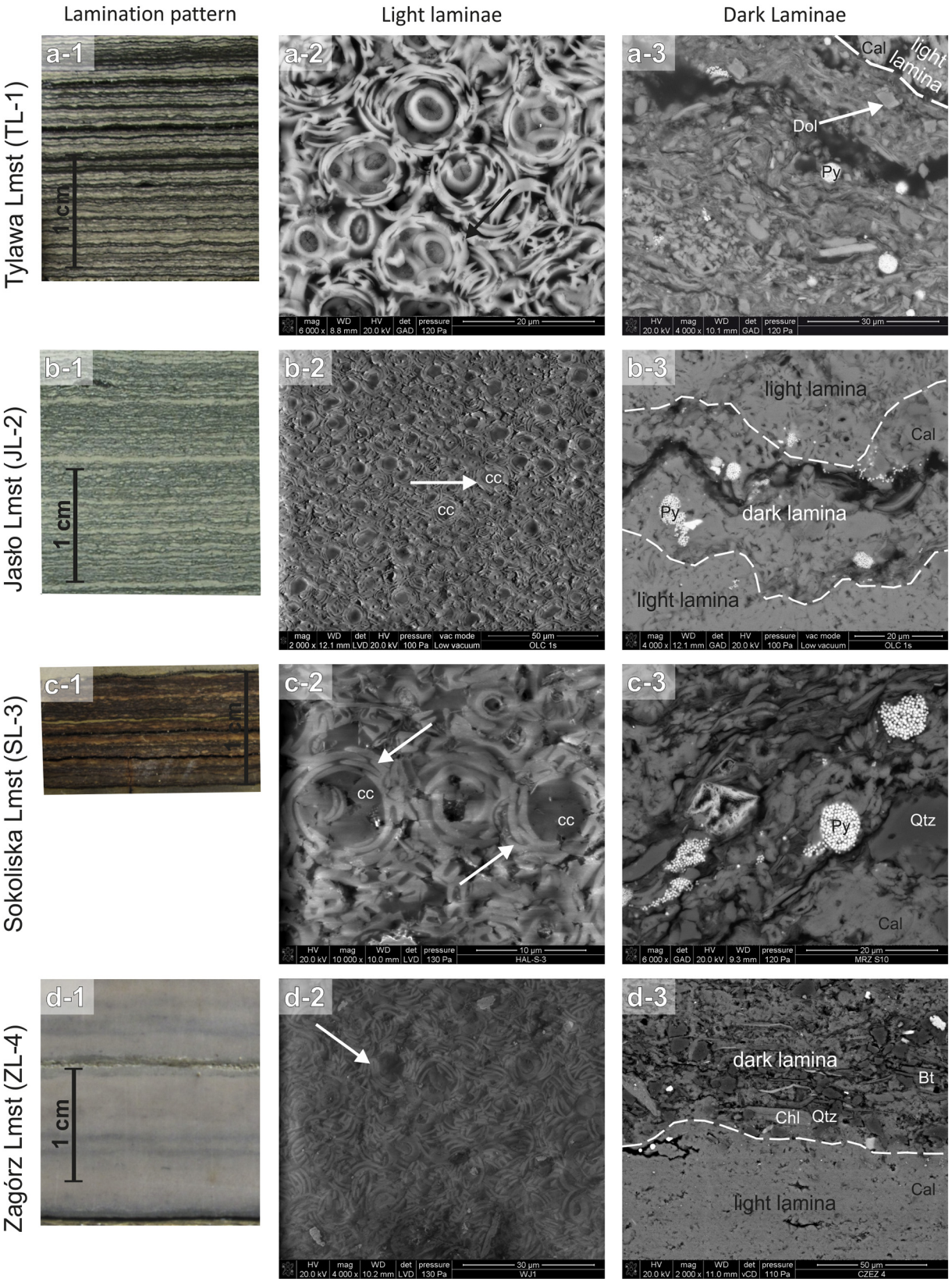

(caption on next page)

Fig. 4. Lamination patterns and composition of the four limestone horizons: a – Tylawa, b – Jasło; c – Sokoliska; d – Zagórz limestones. (a-1–d-1) Macroscopic images of polished sections showing the thick light laminae rich in coccolithophores (a-2–d-2) separated by thinner dark laminae, rich in detrital material (a-3–d-3). Note that the fine lamination and micronodular fabric occur only in TL-1, JL-2 and SL-3 (a-1 – c-1), not in ZL-4 (d-1). (a-2–d-2) SEM images of thin sections showing the abundance of coccolith material with massive accumulations of coccospheres (interfingering of adjacent coccolith plates in some coccospheres indicated by arrows) as the main components of the light laminae. Note the superb preservation of coccoliths (lack of dissolution, overgrowth or compactional flattening) especially in a-2 (sample Fan_T-2A), where even very delicate structure of the central areas of the plates is perfectly preserved and the material is entirely composed of coccoliths. Coccoliths are usually cemented by early-diagenetic, precompactional calcite cement (cc in b-2 and c-2). ZL-4 contains abundant coccoliths as well, but they are rarely arranged in coccospheres (d-2). (a-3–d-3) SEM images of thin sections showing the dark laminae rich in detrital material (quartz - Qtz, feldspars, biotite - Bt, chlorite – Chl, clay minerals – the finest material), framboidal pyrite (Py), carbonate material (calcite – Cal, dolomite – Dol) and organic matter.

bands are up to several millimeters thick and exhibit gradual transitions. They are almost entirely composed of coccolithophores that are moderately to well preserved, but dominated by loose coccolith plates from disintegrated coccospheres (Fig. 4D-2). Signs of dissolution, secondary overgrowth or mechanical fragmentation of coccolithophores occur locally. Only a few distinctive white and up to 2 mm thick laminae are present. Composition (with regard to detrital and skeletal biogenic material) and thickness of these laminae are similar to those in the older horizons. However, they display homogeneous fabric and contain rare pellets. They are separated by submillimetric, dark laminae with composition and fabric analogous to those in the other horizons.

4.2. Organic matter characterization

TOC content of the limestones ranges from 0.1 to 4.0%, whilst TOC of the mudstone sample Asc_J-4 is 7.3% (Table 1). TOC content in TL-1 is significantly higher (mean 2.2%) than in the other horizons (mean for JL-2 and ZL-4 is 1.1 and 0.5%, respectively; one SL-3 sample yielded a 1.3% value). TS content varies from nil to 2.7% in the limestones (with the lowest values in ZL-4), whilst it is 4.1% in the mudstone sample. $\delta^{13}C_{org}$ and $\delta^{15}N_{org}$ values are similar in JL-2, SL-3 and ZL-4 (Table 1). $\delta^{13}C_{org}$ range from −26.4 to −23.4‰ (n = 29) with means for JL-2, SL-3 and ZL-4 being −24.5 (sd = 0.9), −24.8 (sd = 0.2) and −24.9‰ (sd = 0.4‰), respectively. $\delta^{15}N_{org}$ range from 0.2 to 0.8‰ with two outliers at −2.5 and 2.2 in ZL-4 (n = 16) with means for JL-2, SL-3 and ZL-4 being 0.2 (sd = 0.1), 0.3 (sd < 0.1) and 0.2‰ (sd = 2.0‰), respectively. The lower parts of JL-2 in Ascuns and Paltinu sections were sampled with a higher resolution, which revealed that their basal parts exhibit the lowest $\delta^{13}C_{org}$ values of all JL-2 samples. $\delta^{13}C_{org}$ and $\delta^{15}N_{org}$ values of TL-1 are by 2–3‰ and 1–4‰ lower than those of the other horizons, ranging from −29.5 to −24.2‰ (mean − 27.1‰, sd = 1.5‰, n = 10) and from −4.1 to −1.1‰ (mean − 2.1‰, sd = 1.3‰, n = 5), respectively (Table 1). $\delta^{13}C_{org}$ and $\delta^{15}N_{org}$ of mudstones are within the ranges characteristic for the associated limestones, except $\delta^{15}N_{org}$ of TL-1 being significantly ^{15}N-depleted by 1.5–4.5‰ relative to the intercalating mudstones.

Lipid biomarker analyses showed that the sedimentary organic matter is relatively immature in most of the samples. The steranes are dominated by the C_{26}-C_{30} 5α, 22R-steranes and low abundances of 5β-22R-steranes (Fig. 5A). Moreover, where present, hopanes have predominantly the 17β, 21β-stereoconfiguration and are extended up to the C_{37} homologue (sample Bez_T-5A). The stereoconfiguration of the hopanes and steranes indicate low maturity (Peters et al., 2005), which contrasts somewhat with the n-alkane distributions that often show a low odd-over-even predominance (1.2–1.8) and equal abundances of short chain n-alkanes (C_{17}–C_{25}) and long chain n-alkanes (C_{27}–C_{35}). This may indicate that these n-alkanes have a relatively large contribution of marine n-alkanes, rather than the terrestrial ones which generally have a high odd-over-even predominance (> 3; Eglinton and Hamilton, 1963). However, some samples (e.g. WUJ_T-14B) did reveal an odd-over-even predominance indicating an input of terrestrial n-alkanes (Fig. 5B).

The analyses of the apolar fractions revealed also a number of specific lipid biomarkers. The main lipid biomarkers are likely of aquatic origin, but in some cases specific higher plant triterpenoids were detected. For example, high amounts of retene were detected in

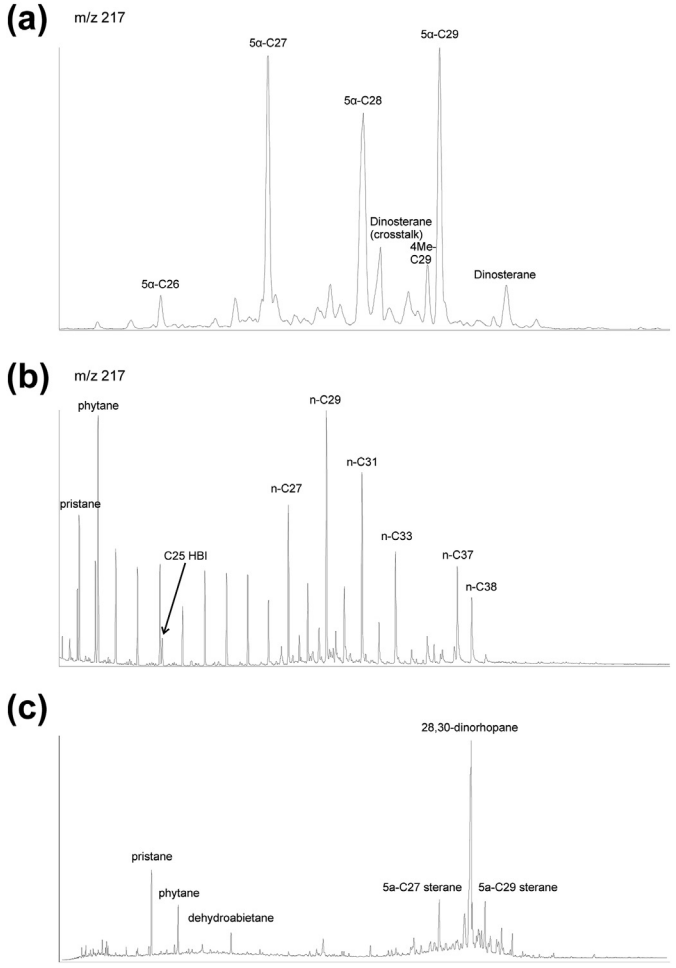

Fig. 5. Three chromatographs depicting typical distribution of lipid biomarkers. **(a)** Mass chromatogram of m/z 217 revealing the distribution of steranes in Tyr_S-4 (SL-3). **(b)** Mass chromatogram of m/z 57 revealing the distribution of alkanes in Wuj_T-14B (TL-1). **(c)** Gas chromatogram of the apolar fraction of Tyr_S-4 (SL-3).

sample Tyr_J-1A, whereas dehydroabietane was detected in sample Tyr_S-4. All these lipid biomarkers indicate conifers as the source (Simoneit, 1986). In selected samples, dinosterane and a C_{29} 4-methylsterane were detected, which are likely of dinoflagellate origin (Boon et al., 1979). Sample Wuj_T-14B exhibits a somewhat exceptional lipid biomarker composition. It contains small amounts of a C_{25} highly branched isoprenoid, which is derived from diatoms (Volkman et al., 1994). Moreover, a relatively high amounts of C_{37} and C_{38} n-alkanes relative to C_{35} n-alkane were detected in this sample. These compounds are likely derived from the haptophyte algal (e.g. coccolithophore) derived long chain alkenones, which may have initially been sulfurized and then released upon diagenesis (Koopmans et al., 1997).

The most striking lipid biomarker was 28,30-dinorhopane which sometimes dominated the apolar fraction (Fig. 5C). It was found in seven samples (out of sixteen) from three horizons; TL-1 is the only one

where this compound was not detected. The 28,30-dinorhopane is often a prominent hydrocarbon in sediments from stratified environments and their derived oils (e.g. Schoell et al., 1992) and can indicate highly reducing to anoxic environments (e.g. Grantham et al., 1980). The C_{28} 28,30-dinorhopane and related aromatic derivatives are likely derived from bacteria dwelling at or below the chemocline and may be used as indicators of stratified water bodies in the past (Sinninghe Damsté et al., 2014).

Pristane and phytane are present in high abundance and the pristane/phytane ratio varies between 1.4 and 3.2. Although this can potentially indicate a relatively oxic environment (Peters et al., 2005 and references therein), this ratio has often been shown not to reflect redox conditions and thus is ambiguous in its use (e.g. Ten Haven et al., 1987; Koopmans et al., 1999).

4.3. C, O and Sr isotope composition of carbonate

Stable carbon and oxygen isotope measurements were performed on bulk carbonate material, so the $\delta^{13}C_{carb}$ and $\delta^{18}O_{carb}$ values (Table 1) represent a mass balance between all the carbonate constituents. $\delta^{13}C_{carb}$ values of samples collected from individual light laminae and from the sets of several adjoining laminae (between −2.7 and 2.8‰) are within the range typical for marine carbonates (Bathurst, 1981). Samples collected selectively from the dark laminae show slightly lower $\delta^{13}C_{carb}$ values (e.g. Fan_T-2C and Fan_T-2D: −2.2 and −2.4‰, respectively) than the adjoining light ones (e.g. Fan_T-2A and Fan_T-2B: −1.8 and −1.9‰, respectively). $\delta^{18}O_{carb}$ values of the limestones are low (between −6.7 and −2.0‰) and always lower than in the intercalating mudstones (up to −1.8‰). Samples that are free of carbonate cements and contain only biogenic carbonate material, chiefly coccoliths, i.e. TL-1 from Fântânele (samples Fan_T-2A and Fan_T-2B) and JL-2 from Wisłok Wielki (samples Wis_J-3A and Wis_J-3B), appear to show increased $\delta^{18}O_{carb}$ values (between −2.5 and −2.0‰). Spreads of $\delta^{13}C_{carb}$ and $\delta^{18}O_{carb}$ values within a given limestone horizon in a single section are both up to 2.0‰. The basal parts of the limestones sometimes exhibit the lowest $\delta^{18}O_{carb}$ values, which is not observed for the $\delta^{13}C_{carb}$. Mean $\delta^{13}C_{carb}$ value for TL-1 is −0.9‰ ($n = 53$), which is significantly lower than those for the other horizons: 1.4‰ ($n = 65$) for JL-2, 1.3‰ ($n = 16$) for SL-3 and 0.9‰ ($n = 40$) for ZL-4. Mean $\delta^{18}O_{carb}$ values for individual horizons are similar, as they range from −4.7 to −4.2‰ (sd < 1.1‰).

$^{87}Sr/^{86}Sr$ ratios of all bulk samples of the limestones (Table 1) are considerably higher than those of the contemporaneous seawater based on the reference sections (Oslick et al., 1994; Reilly et al., 2002) and the LOWESS 5 fit to the marine Sr isotope curve (see McArthur et al., 2012). Because marine $^{87}Sr/^{86}Sr$ values exhibit a constant rise during the Oligocene (Oslick et al., 1994; Reilly et al., 2002), this ^{87}Sr enrichment makes the numerical ages of the limestones erroneously too young. $^{87}Sr/^{86}Sr$ ratios of the limestones were compared to those representing the age of the horizons based on the regression analysis performed by Reilly et al. (2002). 31.2 Ma was set for TL-1 (middle part of the Rupelian), whilst 28.4 Ma for JL-2, SL-3 and ZL-4 (Rupelian/Chattian transition). The minimum ^{87}Sr enrichment (taking into account analytical errors of the measurements that are between 8 and 15×10^{-6}) ranges from 2.1 to 4.4×10^{-4} for the bulk samples, which makes their ages underestimated by at least 5.7 to 11.6 Ma. Apart from these bulk samples, Sr isotope ratio was measured in one light uncemented lamina consisting exclusively of coccoliths (Fan_T-2A), which exhibits ^{87}Sr enrichment as well. However, this enrichment is weaker, as the $^{87}Sr/^{86}Sr$ ratio is by 1.2×10^{-4} higher than that of seawater for 31.2 Ma. This makes the age of this sample underestimated by at least 3.3 Ma. All these ^{87}Sr enrichments and the corresponding underestimation of numerical ages are the minimum values. Application of regression calculated by Oslick et al. (1994) would make these values even greater.

4.4. S isotope composition and size of pyrite framboids

Framboidal pyrite (FP) is the only or the dominant sulfide mineral in the limestones with very rare euhedral pyrite grains. Framboids are usually dispersed in the rock matrix and rarely clustered. Individual framboids are never filled-in. The number of measurements of FP diameters per sample varies from 29 to 5313 (Table 1) and provides only a rough estimation of FP abundance, as the area examined was not equal in all thin sections analyzed. Two sets of samples can be distinguished. The first set comprises twenty samples that contain FPs with very small and relatively invariant diameters (median 3.3–5.0 μm, sd 1.1–1.8 μm). Although almost a half of these samples contain FPs with diameters > 10 μm (up to 27.6 μm), such large aggregates constitute insignificant part (< 0.7%) of all framboids measured. The second set comprises four samples containing FPs with larger (median 4.0–7.5 μm) and more variant diameters (sd 2.0–3.1 μm). Three of them were collected from the basal parts of JL-2 representing initial stages of intensive nannoplankton deposition; one represents ZL-4. The most distinctive feature of the second set of samples is the content of framboids with diameters > 10 μm, which is significantly higher (between 2.1 and 15.2%) than in the first set. The new methodology of semiautomatic FP diameter measurements using SEM and Espirit software turned out to be very efficient. It allowed to collect a very large number of measurements with a high precision and pyrite micromorphologies other than individually dispersed framboids were effectively filtered out.

S isotope measurements were performed on sulfides, which comprise almost exclusively FP. $\delta^{34}S$ values of the limestones (Table 1) are mostly low between −44.0 and −18.5‰ ($n = 31$). However, two samples (Wuj_T-7G and Dyd_Z-7) exhibit significantly higher values of −2.1 and 6.4, respectively. Such values have been recorded neither in JL-2 nor SL-3. Moreover, these horizons exhibit on average lower $\delta^{34}S$ values (mean for JL-2 is −32.7‰; the single sample of SL-3 is −35.0‰) than TL-1 and ZL-4 with mean values of −23.5 and −18.4‰, respectively. $\delta^{34}S$ values of two mudstone samples are within the ranges of the associated limestones.

4.5. Composition and preservation of foraminifera

The distribution of planktonic foraminifera is strongly dependent on the limestone horizon analyzed. They were recorded only in JL-2 and SL-3. SL-3 contains only a single planktonic foraminiferal test identified in sample Buk_S-3. JL-2 is the only horizon rich in planktonic foraminifera. It comprises a low diversity assemblage dominated by globigerinids: *Globigerina praebulloides* Blow - *G. officinalis* Subbotina group with single specimens of biserial planktonic foraminifera *Chiloguembelina gracillima* (Andrae) in Olc_J-0 sample. Foraminiferal shells occur in light and dark laminae, but they are distinctly more abundant in the latter. All shells tend to be distributed outside fecal pellets. Sizes of shells range from 50 to 300 μm in diameter, therefore, larger individuals overlap the size of fecal pellets with diameters in horizontal plane reaching on average ~300 μm. It is supposed that planktonic foraminifera are not a regular part of copepods' diet. In fact, they often prey on small copepods and other crustaceans (e.g., Anderson and Bé, 1976; Hemleben et al., 1989). Preservation of planktonic foraminifera analyzed in cross-sections is usually very good with some traces of dissolution in a single lamina of JL-2, where a few shells are partly dissolved.

Fig. 6 shows the strong covariance ($R^2 = 0.904$) between the abundance of foraminiferal shells and the total number of chambers in all JL-2 subsamples. It indicates that most of the samples, except for a single outlier, consist of in situ assemblages with planktonic foraminifera deposited from pelagic suspension. The abundance of foraminifera in JL-2 usually ranges from 60 to 990 specimens/cm^3 of the sediment (Fig. 6). However, selected lamina sets show much higher variability from 0 or a few individuals up to 2940 specimens/cm^3 in the most productive lamina sets. The average abundance of foraminifers is

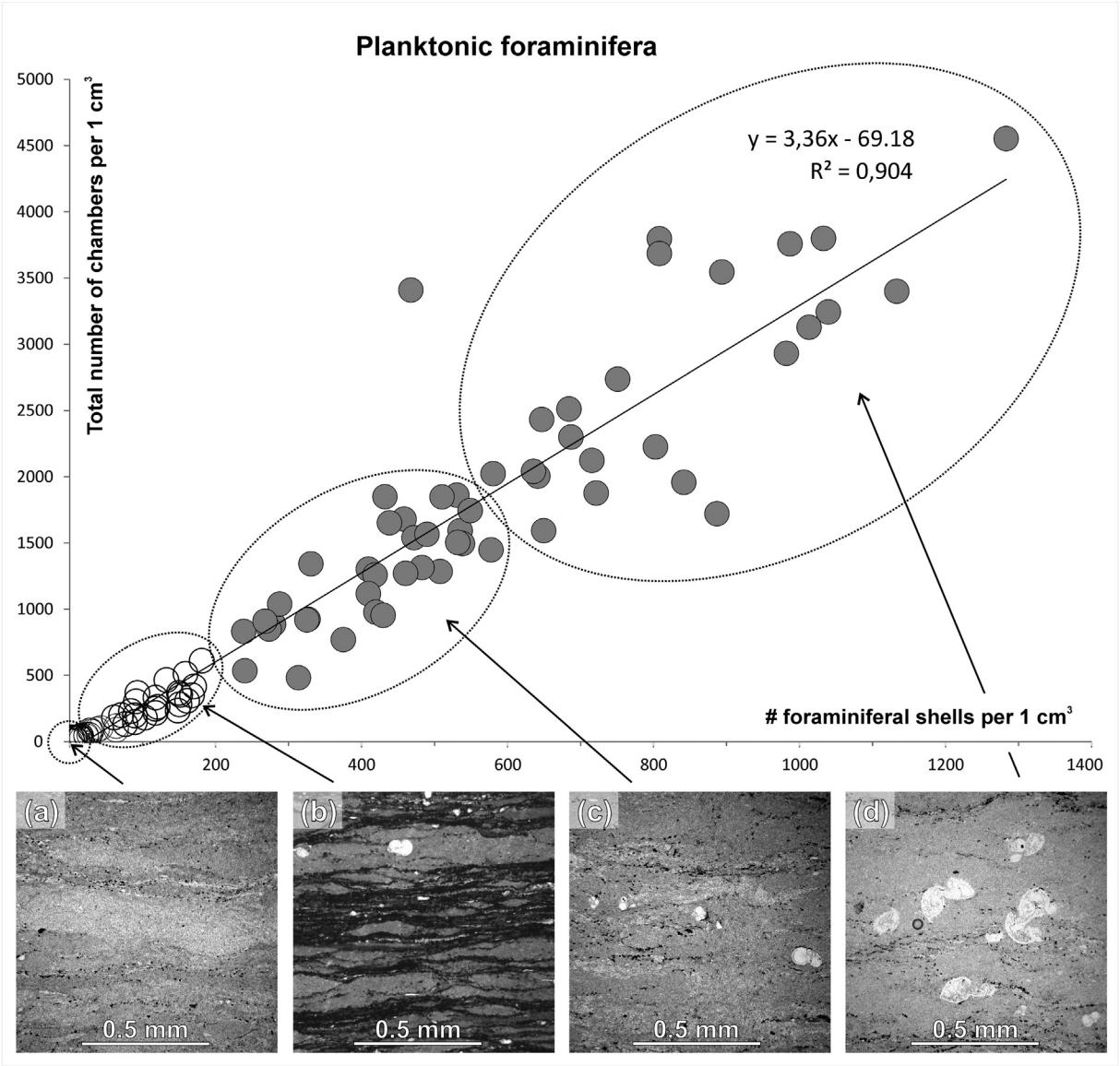

Fig. 6. Diagram showing the linear relation between the number of foraminiferal tests and the total number of their chambers. (a) TL-1 barren of foraminifera. (b–d) three different parts of a single JL-2 sample with different abundance of foraminifera.

around 740 and 780 specimens/cm^3 in the Skole and Silesian basins, respectively. The shells are, however, unevenly distributed, as the highest abundances are recorded in the upper parts, whilst the lower parts of JL-2 show reduced frequencies from 10 to 150 specimens/cm^3. These values suggest either a lower productivity of planktonic foraminifera or a higher dilution by coccolith ooze, therefore a higher productivity of coccolithophores, during the onset of JL-2 deposition. The first interpretation seems to be more likely, because the uniform thickness of the laminae across the JL-2 suggests stable productivity of coccolithophores (see Haczewski, 1989; Ciurej, 2009).

4.6. Composition of palynofacies

The non-palynomorph part of the palynofacies (palynodebris) consists of highly immature, likely marine-derived fabrics, suggesting low maturation state and high marine primary productivity. The palynodebris from evidently terrestrial origin is absent or occurs in very low amounts. Terrestrial palynomorphs are ubiquitous throughout all slides investigated but always in trace amounts only. They were likely strongly diluted by the high input of marine palynofacies. Most pollen found are typically wind-dispersed bisaccate conifer pollen.

Organic-walled dinoflagellate cyst (dinocyst) abundances vary considerably between the four limestone horizons and the intercalating mudstones (Table 1). Merely four specimens of dinocysts were found in two samples (out of seventeen) of TL-1 and the associated mudstones. This may be due to the relatively high sedimentation rates in combination with strong dilution of the dinocysts owing to the immature nature of the sediment and high organic carbon content. The low maturity of the sediment causes the high abundance of amorphous organic matter, which remains after palynological sample processing. The other three limestone horizons are rarely barren of dinocysts, but the counts are relatively low. The dinocysts that are present, include a low-diversity assemblage with *Deflandrea phosphoritica*, *Homotryblium* spp., *Distatodinium paradoxum, Thalassiphora pelagica* and occasionally *Selenopemphix nephroides*. High abundance of *Homotryblium* indicates strong surface water stratification, while the abundance of *Selenopemphix*, *Deflandrea* and *Brigantedinium* are indicative of (at least seasonally) high nutrient availability (Table 1). JL-2 and ZL-4 are especially rich in these taxa (Table 1). However, several samples contain a less restricted, more normal marine assemblage, suggesting that variability in the severity of

runoff-induced stratification relative to the marine influence must have occurred. This assemblage is especially abundant in SL-3.

5. Discussion

Up to four lithological units can be distinguished in the Holocene Black Sea sediments (Jones and Gagnon, 1994; Lyons, 1991; Arthur and Dean, 1998). The Pleistocene-Holocene transition is recorded in organic C-poor (< 1%), massive clays of Unit III deposited in an oxic freshwater lake. At ~7.9 ka deposition of organic C-rich (< 20%), carbonate-poor, finely laminated sapropel (Unit II) commenced, which roughly coincides with a shift to marine anoxic conditions. At ~2.7 ka the sea was invaded by a coccolithophorid *Emiliana huxleyi* and the rate of detrital input increased without a change in organic matter supply rate, which changed sedimentation to finely laminated, coccolith marls with 10–75% of carbonate and 1–5% of organic C content (Unit I). Homogeneous turbiditic muds, representing redeposited siliciclastic shelf material, are often found interbedded with Units I and II in the deep parts of the basin.

The Oligocene rocks in the Central Paratethys can be considered as ancient counterparts of the recent Black Sea sediments with regard to TOC contents, petrographic and sedimentological properties. The finely laminated coccolith limestones herein examined with TOC < 4% correspond to Unit I sediments, the black finely laminated organic C-rich (TOC < 18%, Köster et al., 1998a; Kotarba and Koltun, 2006) shales correspond to sediments of Unit II, whilst fine-grained turbidites correspond to the muds intercalated with Units I and II. Below, biotic and geochemical characteristics of the Oligocene coccolith limestones from the Central Paratethys are compared with those of the present-day Black Sea and its recent sediments with respect to the major environmental conditions.

5.1. Bottom water anoxia

Euxinic conditions (anoxic and sulfidic) in the distal parts of the Black Sea stretch from the sea bed at > 2000 m to the euphotic zone at about 100–150 m b.s.l., whilst well-oxygenated surface water reaches 50–100 m b.s.l. (Codispoti et al., 1991). Up to 50 m thick intermediate suboxic layer, almost free of both O_2 and H_2S, is developed between them (Murray et al., 1989; Jensen et al., 2008). The Oligocene limestones analyzed here, are usually finely laminated and generally undisturbed by burrowing, which indicates anoxic conditions in the bottom waters of the Central Paratethys. Rather simple and poor assemblages of trace fossils were found only in JL-2 in several sections. They include *Trichichnus* and *Multina* suggesting that short periods when oxic/dysoxic conditions alternated in bottom waters locally (Kotlarczyk and Uchman, 2012). Benthic fauna is also very rare in the limestones (see Bieńkowska-Wasiluk, 2010, and references therein) and may have been redeposited from proximal settings. Only five calcareous benthic foraminiferal tests were identified in a single sample of SL-3 (Tyr_S-10) in this study. These single indistinguishable specimens are relatively well preserved, but have tiny tests with 1 to 3 crosscut chambers. Agglutinated foraminifers have never been observed in the investigated thin sections, therefore, these tiny tests may represent unsuccessful colonization of anoxic floor by meroplanktonic juvenile individuals (see Alve, 1999). Fish fossils are quite common in the Oligocene series, but their preservation state is better in the coccolith limestones, especially in TL-1 (Bieńkowska, 2004), than in the mudstones (e.g. Kotlarczyk et al., 2006), probably due to bottom-water anoxia (Bieńkowska-Wasiluk, 2010). Moreover, TL-1 contains an unusual ichthyofaunal assemblage characterized by elimination deep-water taxa, which is interpreted as a result of oxygen minimum zone reaching as high as 500 m b.s.l. (Kotlarczyk et al., 2006).

Yet, the upper water column was inhabited by shallow-water fishes (Kotlarczyk et al., 2006) and the photic zone was densely populated by coccolithophorids and crustacean nekton (e.g. copepods), as documented by fecal pellets packed with coccoliths, which confirm relatively well oxygenated upper water column (0–50 m). Among planktonic foraminifera (when present in JL-2 and SL-3), deeper water (down to 400 m) species do not occur, which suggests that the chemocline was positioned relatively high in the water column. However, these species hardly tolerate decreased salinity (Bijma et al., 1990) and their juvenile forms dwell in the shallowest part of water column, which was certainly brackish in the basin (see section 5.3). Hence, their absence may equally result from decreased salinity. Still, stratification in the water column is confirmed by a low-diversity dinoflagellate assemblage with *Homotryblium* spp. Interestingly, TL-1 is the only coccolith limestone horizon which is almost barren of dinoflagellates. However, this may be related with the very high content of amorphous organic matter diluting the dinoflagellates, not necessarily with any particular paleoenvironmental condition.

These biotic and sedimentological indices suggest that anoxic conditions developed below and well above the sediment-water interface. This is supported by the size distribution and $\delta^{34}S$ values of framboidal pyrite (FP). Although FP may be formed abiotically (e.g. Berner, 1969; Sweeney and Kaplan, 1973; Wilkin and Barnes, 1996), a bacterial origin for the FPs in the limestones examined is confirmed by their low $\delta^{34}S$ values (between −44 and −18.5‰). The lower part of this range corresponds to the present-day $\delta^{34}S$ of sulfide dissolved in the anoxic water column (from −42 to −32‰; Sweeney and Kaplan, 1980; Fry et al., 1991; Neretin et al., 2003), to the currently sedimenting iron sulfides (from −40 to −32‰; Muramoto et al., 1991) and to FP in the surface coccolith ooze (Unit I) in the Black Sea (from −38.3 to −33.6‰; Calvert et al., 1996; Jørgensen et al., 2004), whilst the upper part to $\delta^{34}S$ of FP in the sapropel layer (Unit II; ≤22‰; Calvert et al., 1996; Wilkin and Arthur, 2001). These generally low values show that sulfate reduction and precipitation of iron sulfides was mediated by microbial activity, as bacteria preferentially utilize the lighter sulfur isotope during reduction of sulfate (Chambers and Trudinger, 1979; Bottrell and Raiswell, 2000; Canfield, 2001). The shift of $\delta^{34}S$ values from marine sulfate to H_2S during bacterial sulfate reduction (BSR) reported from culture studies can be up to ~47‰ (Chambers et al., 1975; Chambers and Trudinger, 1979; Detmers et al., 2001; Habicht and Canfield, 2001). Considering that marine sulfate was isotopically heavy (~22‰) during Oligocene (Paytan et al., 2011), the difference in $\delta^{34}S$ between pyrite and seawater sulfate (< 66‰) exceeds the maximum possible shift in $\delta^{34}S$ related to the fractionation effect during BSR. However, in anoxic marine basins only some part of sulfide produced in the water column by BSR is precipitated as metal sulfides, sinks to the seafloor and can be buried, whereas a large part of hydrogen sulfide is reoxidized at the chemocline producing sulfate and sulfur species with intermediate oxidation states (Jørgensen, 1982). These intermediate S species undergo bacterial disproportionation, which is associated with a strong S isotope fractionation leading to production of extremely ^{34}S-depleted sulfide (see Canfield and Thamdrup, 1994; Habicht et al., 1998; Böttcher et al., 2001; Bottrell and Newton, 2006). These processes have also taken place in the water column of the Black Sea during the last 2.7 kyr and are responsible for the lowest $\delta^{34}S$ values of FP in Unit I sediments (Lyons, 1997) and sulfide currently dissolved in the anoxic water column (Neretin et al., 2003). We believe that a similar mechanism must be responsible for the lowest $\delta^{34}S$ values recorded in the limestones examined.

The size and distribution of bacterially-formed FPs is a proxy for redox conditions (Wilkin et al., 1996; Wignall and Newton, 1998). Syngenetic FP formation within the water column related to anoxic conditions is associated with a homogeneous distribution of small-size framboids within the sediments, except the preferential occurrence in microfossils related to the localized decay of organic matter. Dominance of larger framboids, often heterogeneously distributed as clusters (Böttcher and Lepland, 2000), is linked to diagenetic formation at the redox interface located within the sediments. In the Black Sea sediments deposited during the last 7.5 kyr (Units I and II) when

permanent bottom water anoxia have existed, FP diameters are very small and invariant (mean of 5 μm with > 95% of FP < 7 μm; Wilkin et al., 1997), which is similar to our data. FPs are evenly distributed in all four limestone horizons examined and exhibit uniform and small sizes with diameters rarely > 10 μm (up to 0.7%), median values from 3.3 to 5.0 μm and sd values up to 1.8 (Table 1). This clearly shows that the framboids are syngenetic and that the bottom water was anoxic.

Only one sample (Pal_J-4A) contains considerably larger framboids with a median diameter of 7.5 μm and 15.2% of framboids with diameters > 10 μm. This sample is not laminated and was apparently deposited under oxic conditions and iron sulfides formed diagenetically within the sediments. Three other samples (two from JL-2, one from ZL-4) contain predominantly very small framboids, but exhibit slightly increased content of framboids > 10 μm (2.1–3.8%) which is manifested by higher sd values between 2.0 and 2.6 μm. The presence of 28,30-dinorhopane (discussed below), undisturbed fine lamination and lack of benthic fauna in these samples confirm water-column stratification during their deposition, which indicates that FP formed mostly in the water column with a small addition of diagenetic pyrite.

The presence of 28,30-dinorhopane in JL-2, SL-3 and ZL-4 confirms that the water column was stratified with respect to oxygen level. The absence of 28,30-dinorhopane in some samples and in TL-1 does not mean that there was no anoxia or stratification. Plenty of sediment records have anoxia indicated by isorenieratane, a specific lipid biomarker for photosynthetic green sulfur bacteria or its derivatives (Koopmans et al., 1996), whilst lacking 28,30-dinorhopane, e.g. in the Holocene Black Sea sediments (Huang et al., 2000). However, we did not detect isorenieratane in any sediment nor did we detect any organic sulfur compounds, compounds formed under anoxic sulfidic conditions (Sinninghe Damsté et al., 1989). Considering the immature nature of the sediment, isorenieratane should have rather been preserved, if sulfide production occurred close to the photic zone (Summons, 1993). It is evident that anoxicity existed in the water column and that sulfide was produced in the lower water column in the Paratethys, as indicated by the abundance, size and S isotope composition of FP. Thus, euxinic conditions did not reach the photic zone, which is unlike the Black Sea, where photic-zone euxinia has persisted permanently in the central part of the basin during the deposition of Unit I (Sinninghe Damsté et al., 1993; Huang et al., 2000). TL-1 is the only horizon that does not contain 28,30-dinorhopane, which makes it similar to the recent coccolith marls in the Black Sea where this compound was not identified as well.

The coincidence of several exceptional features of TL-1 (the lowest content of FP with diameters > 10 μm, the highest TOC content, fine and continuous lamination, absence of trace fossils, absence of deep-water fishes) suggests that anoxia was permanent and that the basin was more anoxic than during sedimentation of the other horizons. Organic matter was less efficiently oxidized during settling due to the thicker layer of anoxic bottom waters. Still, euxinic conditions likely did not reach the photic zone, as isorenieratane was not detected. ZL-4 is the only horizon that does not show micronodular fabric and is poor in zooplankton fecal pellets. Therefore, organic matter was less protected during settling through the oxic water column than in the case of other horizons. This is probably the cause of lower TOC and TS contents in ZL-4 than in the other horizons.

5.2. Preservation of original pelagic carbonate material

Coccoliths are the main carbonate component of the studied limestones. They are well preserved in all horizons and usually show all morphological features intact. They often occur as complete, perfectly spherical coccospheres (Fig. 4) except the youngest horizon (ZL-4), where they are mostly disseminated as individual plates (Fig. 4D-2). Still, coccoliths in all horizons are only slightly modified by diagenetic processes. They exhibit little evidence of partial dissolution in some samples of TL-1, JL-2 and SL-3, which might have occurred before sedimentation, probably due to digestive processes of zooplankton or in the water column. Recrystallization features have not been observed in any sample despite the fact that some of the limestones (from the Dukla and Silesian units) were deeply buried to the oil window conditions (Köster et al., 1998a; Kotarba and Koltun, 2006). Moreover, oxygen isotope ratios did not undergo secondary resetting, which is demonstrated by the lack of linear correlation between $\delta^{13}C$ and $\delta^{18}O$ values and by the broad range of $\delta^{18}O$ values (3–4‰ for each limestone horizon and < 2‰ for a horizon in a single outcrop). A late diagenetic resetting of $^{18}O/^{16}O$ would have otherwise led to unification of $\delta^{18}O$ values (Bojanowski et al., 2014). This fact and the exceptional preservation of calcareous nannoplankton indicate that the carbonate material in samples without carbonate cements, i.e. Fan_T-2A, Fan_T-2B, Wis_J-3A and Wis_J-3B, represents unaltered coccolith oozes. Therefore, their carbonate geochemical properties provide direct and reliable record of paleoenvironmental conditions in the photic zone where calcification of nannoplankton occurred and provide insight into paleoceanographic conditions during their deposition. Composition and preservation of these limestones resemble those of the pelagic ooze being currently deposited in the Black Sea.

In other samples, carbonate cementation was the only diagenetic process that could have affected the properties of their carbonate material. The material in the light laminae is usually cemented with calcite, which never predominates over coccoliths, but constitutes rather minor amount of bulk carbonate (presumably < 20%). This calcite envelopes coccospheres or foraminifers, which show excellent preservation and are seldom flattened. This suggests that calcite precipitation took place prior to significant mechanical compaction, thus, very close to the sediment-water interface, within up to several decimeters or meters of sediments (see Bennett et al., 1991; Burdige, 2006), from pore fluids representing at most insignificantly altered basin water. Presence of such extremely early calcite cements does not necessarily preclude application of stable isotope analysis of nannoplankton-dominated carbonate sediments as a paleoenvironmental proxy, as evidenced by Bojanowski et al. (2017), provided that bicarbonate dissolved in the interstitial fluids was not liberated by microbial modifications of organic compounds causing strong isotope fractionation (e.g. Bojanowski, 2012). Indeed, $\delta^{13}C$ values of the limestones (Table 1) are within the range for unaltered marine carbonates and do not seem to be noticeably modified by calcite cementation. However, the uncemented samples of TL-1 and JL-2 clearly exhibit the highest $\delta^{18}O$ values among all (Table 1), which suggests that presence of calcite cement drives $\delta^{18}O$ of the limestones to slightly lower values.

Fe-rich dolomite is present as individual rhombohedra dispersed mostly among the siliciclastic material in the dark laminae, so dolomitization did not affect the biogenic carbonates. The dark laminae containing dolomite show only slightly different $\delta^{13}C$ (by 0.5‰ lower) and $\delta^{18}O$ values (by 0.2‰ lower) than the adjacent light ones composed exclusively of coccoliths in sample Fan_T-2 (Table 1). This difference is even less significant in other samples. This dolomite cement does not have an important impact on the isotopic composition of the limestones, as it contributes insignificant amount of carbonate to bulk material (presumably < 1%; except two dolomitized samples from Romania, which were excluded). Thus, bulk isotopic composition of the limestones corresponds to the composition of calcareous nannoplankton with possible minor signal from calcite cement, which never constitutes a major part of the carbonate material. Therefore, the geochemical properties of the carbonate fraction of the limestones chiefly reflect paleoceanographic conditions in the photic zone during their deposition with possible little post-depositional overprinting related to extremely early diagenesis.

5.3. Basin restriction and fresh water supply

Paleotemperature calculations (Appendix) yielded unreasonably high values (< 54 °C; mean > 40 °C) for all limestone horizons (Table 1). Even paleotemperatures calculated for samples without

carbonate cements, i.e. Fan_T-2A, Fan_T-2B, Wis_J-3A and Wis_J-3B are clearly too high (from 28 to 31 °C) as for marine sea-surface temperatures (SSTs) in mid latitudes and temperate climate conditions characteristic for the Oligocene ice-house period (Miller et al., 1991; Zachos et al., 1993). For instance, SSTs were < 30 °C in equatorial regions (Tremblin et al., 2016), whilst they merely reached 20 °C in high latitudes (Liu et al., 2009) around 30 Ma. In the Paratethys, the Eocene-Oligocene transition was associated with a major climatic cooling reflected in a drastic shift from warm-water nummulitic assemblages that recorded SST between 20 and 25 °C (Sótak, 2010) to cold-water biota (Olszewska, 1998; Gedl, 2000). Moreover, examinations of floral assemblages indicate mean annual air temperatures of 15–17 °C in the circum-alpine region during the Early Oligocene (Bruch, 1998). Therefore, it is clear that the Paratethys basin water was depleted in ^{18}O relative to contemporaneous ocean water, which was recorded in these low $\delta^{18}O$ values of the coccolith limestones.

Further evidence of basin restriction comes from Sr isotope data. The $^{87}Sr/^{86}Sr$ values are significantly higher than those of contemporaneous seawater for all limestone horizons, which could be explained by carbonate cementation, as even early-diagenetic pore water may exhibit higher Sr isotope ratio than the associated seawater due to interaction with Rb-rich clay (e.g. Steuber et al., 1987). However, ^{87}Sr enrichment is noted also in the uncemented light lamina exclusively composed of coccoliths (sample Fan_T-2A; Table 1), which clearly shows that the basin water in the photic zone was originally enriched in ^{87}Sr. The magnitude of this enrichment relative to the contemporaneous marine $^{87}Sr/^{86}Sr$ value in all the samples analyzed ranges from 1.2 to 4.4×10^{-4} (with the lower limit value obtained for the uncemented sample Fan_T-2A), which is larger than expected for rocks even with a high Rb/Sr ratio related to high contents of clay minerals (see Banner, 1995).

There is no evidence for extensive hydrothermal or volcanic activity in the basin during Oligocene, so the most probable cause of this ^{87}Sr enrichment is significant input of riverine water flowing from areas composed of silicate-rich crystalline rocks that are the main source of the radiogenic ^{87}Sr isotope. Still, significant enrichment in ^{87}Sr in basin water could have occurred only if the basin was efficiently isolated from the open ocean and the water exchange was limited, as in the Black Sea today. Indeed, restriction and freshening of Paratethys during Oligocene was suggested by Melinte (2005) and Švábenická et al. (2007) on the basis of micro- and nannofossil assemblages. Similarly, restriction and high riverine input to the Black Sea, chiefly from the Danube river, are the causes of $^{87}Sr/^{86}Sr$ deviation of current basin water from the marine water inflow from the Aegean Sea with $^{87}Sr/^{86}Sr$ coinciding with that of the global ocean water (Major et al., 2006; Kuznetsov et al., 2012). The magnitude of this deviation (2×10^{-4}; Major et al., 2006; Kuznetsov et al., 2012) is comparable to that of the limestones examined ($1.2–4.4 \times 10^{-4}$). However, the Danube river carries fresh water with a $^{87}Sr/^{86}Sr$ ratio that is lower than that of ambient seawater, as the main sources of Sr in the Danube catchment are currently Mesozoic and Cenozoic limestone-rich sedimentary series (Pawellek et al., 2002). It is assumed that the crystalline basement comprised the main kind of bedrock that was drained during the Oligocene, which caused the radiogenic Sr composition in the Paratethys, as recorded in the coccolith limestones examined. The following rise of the Alpine-Carpathian-Dinaric orogenic system and the associated intensive deposition in extensive foredeep and intramonatne basins covering large areas composed of the crystalline basement must have diminished the role of crystalline rocks in the region and the Sr isotope composition of the rivers switched to unradiogenic.

Restriction of the Paratethys was related to deterioration of ocean water inflow or complete closure of the gates connecting the basin with the ocean. The onset of uplift of the Alpine-Carpathian-Dinaric orogenic system during the Early Oligocene (Báldi, 1984; Tari et al., 1993; Rögl, 1998; Kováč et al., 2016) and/or eustatic sea-level falls could have been responsible for the isolation of the basin. The latter is supported by the fact that significant sea-level falls corresponding to isotopic events occurred at ca. 31.5 and 28.5 Ma (Pekar et al., 2003; Haq and Al-Qahtani, 2005; Miller et al., 2005; Kominz et al., 2008), which is shortly before the deposition of TL-1 and the other horizons, respectively.

Basin restriction explains the abnormally low $\delta^{18}O$ values of the coccolith limestones, as meteoric water, which is significantly depleted in ^{18}O relative to seawater, contributed a large part of basin water. The spread of $\delta^{18}O$ values for a given limestone horizon collected in a single section (up to 2.0‰) may be related to temporal salinity and temperature fluctuations in the basin water. Salinity fluctuations can also explain the strong variability of concentration of planktonic foraminifera, which can hardly tolerate low salinity conditions. Only few species can survive salinity below 30‰ in modern oceans. The salinity tolerance of extant planktonic foraminifera are verified based on culture experiments and ranges from 22‰ to 49‰ (Hemleben et al., 1989; Bijma et al., 1990). This is a maximum range of salinity tolerance of a single species, *Globigerinoides ruber* (d'Orbigny) that was able to construct chambers, calcify, and undergo gametogenesis. Other species have slightly narrower tolerance to salinity from 22–27‰ to 40–49‰ (Bijma et al., 1990). However, a complete life cycle of planktonic foraminifera has never been observed in culture conditions (Hemleben et al., 1989). In situ sampling of surface water planktonic populations in recent ocean shows a smaller range, e.g. Spero and Williams (1990) observed that the lower limit of salinity for *Orbulina universa* to grow its shell was 4.5‰ below ambient in seasonal low-salinity surface waters of the Gulf of Mexico over the last 16,000 years that was still well above its physiologic salinity limit, i.e. 22‰ according to Bijma et al. (1990). Based on these observations and interpretations, we can estimate that a realistic lower salinity range for low diversity populations of planktonic foraminifera starts at about 22–25‰.

We can use this actualistic approach to estimate paleosalinity limits in the studied paleoenvironment, assuming that other controlling factors had no impact on distribution of planktonic foraminifera. Anoxia could eliminate planktonics from the upper water column. Nevertheless, this was not the case because the uppermost water column was well-oxygenated (see section 5.1). As discussed in section 5.2, the taphonomic bias is also not the case, because perfect preservation of coccoliths precludes significant destructive dissolution during diagenesis. Moreover, the absence of planktonic foraminifera in TL-1 cannot be related to dissolution during settling of the tests, as they were exposed to well-oxygenated water for a shorter time than during deposition of JL-2 (rich in planktonic foraminifera), when the chemocline was positioned at a greater depth. The shorter residence in oxic environment should rather enhance the preservation of carbonate microfossils in TL-1. Therefore, we can trust that TL-1 and ZL-4 that are packed with coccoliths, but do not contain any foraminifera, were mostly deposited above the lower salinity limit of coccolithophores (17‰) and below the lower salinity limit of planktonic foraminifera (22‰). These estimates correspond well to the current salinity in the Black Sea surface water (barren of foraminifera) which varies between 16 and 20‰ (Özsoy and Ünlüata, 1997; Tuzhilkin, 2008). Single specimens of planktonic foraminifera in SL-3 may indicate higher salinity limits, up to 25‰, which is already higher than in the Black Sea today. Such salinity reconstructions are broadly consistent with the dinoflagellate cyst assemblages, which contain goniodomid species strongly affiliated to extreme, restricted environments. JL-2 is an exception, as it is the only horizon rich in low diversity planktonic foraminiferal assemblages. The highest abundances recorded in the upper part of JL-2 indicate slightly hypohaline conditions that may be estimated at 28–30‰. The lower part of JL-2 suggests lower salinities (25–28‰). Nannoplankton assemblages display low species diversity with high productivity in all limestone samples investigated. This may be associated with stressful environmental conditions with seasonally variable salinity and, thus, the observed assemblages may represent groups with different salinity tolerances.

Two samples from TL-1 and ZL-4 contain framboidal pyrite with

$\delta^{34}S$ values of −2.1 and 6.4‰ that are significantly higher than those of the rest of the samples. Similarly high $\delta^{34}S$ values of pyrite have been noted in the Black Sea sediments (from −3 to 17‰), but only in the limnic Unit III (Calvert et al., 1996; Wilkin and Arthur, 2001), which cannot be taken as an analog for the coccolith limestones examined. Such high values of syngenetic pyrites indicate that H_2S was produced in the water column by BSR of sulfate significantly enriched in ^{34}S. This enrichment could have been achieved in a restricted basin, if the sulfate pool became significantly replenished due to the rate of sulfate consumption exceeding the rate of supply (Zaback et al., 1993; Lyons et al., 2000). Then, ^{34}S enrichment occurred in the residual sulfate pool that was brought close to exhaustion (cf. Gomes and Hurtgen, 2015). This closed-system Raleigh isotope effect could have been attained only when sulfate reservoir in the basin was especially insignificant. Low sulfate concentration is confirmed by the coincidence of the highest ^{34}S-enrichment and the lowest FP count in sample Dyd_Z-7A-C, which was examined for the FP size distribution (Table 1). The cause of low sulfate concentration was a significant input of fresh water being normally much poorer in sulfate than seawater. The ^{34}S-enriched pyrite and absence of foraminifera in TL-1 and ZL-4 may be genetically linked, which would also suggest that salinity was distinctively lower during the deposition of these horizons than in the case of JL-2 and SL-3. Mean $\delta^{18}O$ values for all samples of a given horizon support this interpretation, as TL-1 exhibits the lowest (−4.2‰), while JL-2 the highest value (−4.6‰). Such extremely low-salinity events when sulfate became strongly depleted could have occurred during periods of perfect isolation of Paratethys from the ocean, which is unlike the Black Sea during the last 7.5 kyr.

5.4. High productivity

$\delta^{13}C_{org}$ values of JL-2, SL-3 and ZL-4 are relatively high (mostly between −26 and − 23‰) indicating a mixture of marine and terrestrial organic matter (Meyers, 1994). Notably, the high values suggest enhanced marine paleoproductivity, as land plant-derived organic matter with $\delta^{13}C_{org}$ values close to −28‰ is normally the predominant organic material of the Oligocene mudstones in the Paratethyan basins (Köster et al., 1998a; Schulz et al., 2005; Bechtel et al., 2012). $\delta^{13}C_{org}$ values of recent sediments in the deep parts of the Black Sea vary similarly between −26 and − 22‰ (Çoban-Yıldız et al., 2006; Quan et al., 2013). Causes of the lower $\delta^{13}C_{org}$ values in TL-1 are discussed in chapter *5.5*. The fact, that TOC content of the modern laminated coccolith marl (Unit I) of the Black Sea (2–6%; Calvert and Karlin, 1998) is higher than that in the limestones examined (< 4%), does not exclude high paleoproductivity in the Central Paratethys, as some part of OM was likely removed during diagenesis.

N isotope composition of bulk organic matter ($\delta^{15}N_{org}$) is also a sensitive proxy for paleopaleoproductivity. The increased riverine input must have driven the surface water $\delta^{15}N$ of bioavailable N to higher values, as particulate organic nitrogen and dissolved nitrate in rivers are typically enriched in ^{15}N by up to several permille (Owens, 1987; Reschke et al., 2002). $\delta^{15}N_{org}$ values of JL-2, SL-3 and ZL-4 are mostly between 0 and 1‰, which suggests that the other source of organic nitrogen was relatively depleted in ^{15}N. Microbial N fixation is the major source of biologically available nitrogen in the oceanic budget (Wada and Hattori, 1990) and is associated with a ^{15}N depletion producing $\delta^{15}N_{org}$ values by < 3‰ lower than that of atmospheric N_2 (Karl et al., 1997; Haug et al., 1998; Sachs and Repeta, 1999). Slightly positive $\delta^{15}N_{org}$ values, similar to those obtained in this study, are commonly associated with increased N fixation (Sachs and Repeta, 1999; Reschke et al., 2002). Therefore, these low $\delta^{15}N_{org}$ values could be associated with a high rate of microbial N fixation prevailing over that of continental input to the surface water of the Central Paratethys. The assumed fast N fixation related to enhanced primary productivity was probably related to intensive phytoplankton blooms in the photic zone (see Sachs and Repeta, 1999), which is in line with the observed coccolithophorid and dinoflagellate assemblages. Similarly, increased anoxia was also considered by Quan et al. (2013) as responsible for the decreased $\delta^{15}N_{org}$ values in recent Black Sea sediments. Moreover, the anoxic bottom water must have been normally stagnant, as upwelling would have otherwise transferred large amounts of isotopically heavy nitrate to the surface waters (Brandes et al., 1998; Ganeshram et al., 2000). Increased surface-water paleoproductivity was also reported for various parts of the Paratethys during Oligocene by others (Köster et al., 1998a; Schulz et al., 2005; Sótak, 2010; Bechtel et al., 2012) and related with the inflow of nutrient-rich fresh-water that caused brackish conditions and water-column stratification in the basin.

TL-1 exhibits on average by ~2‰ lower $\delta^{15}N_{org}$ values than the other horizons and the highest TOC values among them. These extremely low $\delta^{15}N_{org}$ values in TL-1 are significantly lower than those measured in recent Black Sea sediments (~3‰; Fry et al., 1991; Reschke et al., 2002; Quan et al., 2013) and cannot be solely linked to even exceptionally strong surface-water eutrophication (see Sachs and Repeta, 1999; Möbius et al., 2010). Instead, they suggest an additional, strongly N fractionating pathway that produces $\delta^{15}N_{org}$ < 0‰. For instance, ^{15}N-depleted OM (with $\delta^{15}N_{org}$ of −5‰) has been found to form at the top of the anoxic water body in the deep parts of the Black Sea (Çoban-Yıldız et al., 2006). Production of this ^{15}N-depleted biomass in the Black Sea can be attributed to chemoautotrophic bacterial activity (Fry et al., 1991; Çoban-Yıldız et al., 2006) or fixation of N_2 or N_2O that was released by denitrification or annamox (Kuypers et al., 2003; Westley et al., 2006). Interestingly, ^{15}N-depletion has recently been observed in chemosynthetic microbial mats (with $\delta^{15}N_{org} \geq 3.6$‰) that are associated with methane seepage (Levin and Michener, 2002) and TL-1 was deposited during widespread methane venting in the basin, as discussed in chapter *5.5*. However, it does not appear plausible that this mechanism is responsible for the distinctively lower $\delta^{15}N_{org}$ values of TL-1 relative to the other horizons. Instead, it was the thicker layer of anoxic water developed due to stronger anoxic conditions that caused extremely abundant production of ^{15}N-depleted OM in the water column, as it occurs in the Black Sea today (Çoban-Yıldız et al., 2006). Because microbially-formed OM undergoes amorphization (Pacton et al., 2011) the newly formed bacterial OM in the euxinic water column must have contributed to increased deposition of amorphous OM. We speculate that this process can be attributed to the high content of amorphous OM in TL-1, which significantly diluted palynofacies.

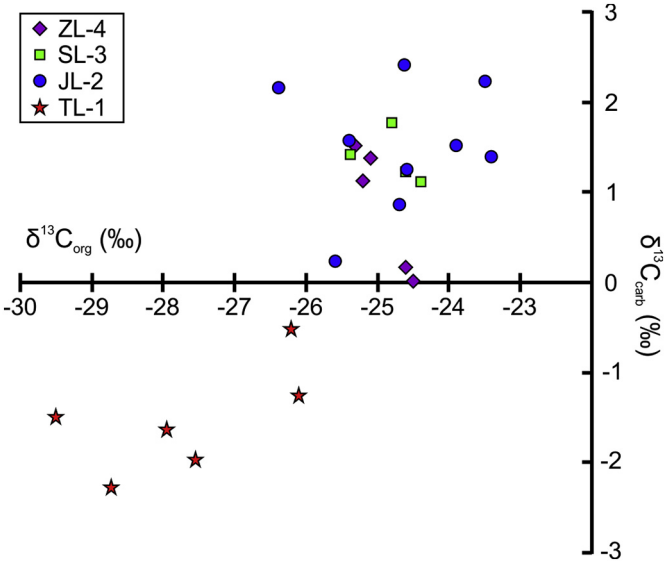

Fig. 7. Plot of $\delta^{13}C_{carb}$ vs. $\delta^{13}C_{org}$ values for all coccolith limestone horizons.

Table 2
Comparison of major conditions between the present-day Black Sea and Central Paratethys during Oligocene.

	Black Sea (since 2.7 ka)	Central Paratethys (Oligocene)	Proxies (this study)
Bottom-water anoxia	YES	YES	Biomarkers, dinoflagellates, lamination, absence of benthic fauna and bioturbation, size of FP
Anoxia in the photic zone	YES	NO	Biomarkers
Bottom-water euxinia	YES	YES	Abundance, size and $\delta^{34}S$ of FP
Brackish conditions	YES	YES	$\delta^{18}O_{carb}$, $^{87}Sr/^{86}Sr_{carb}$, planktonic foraminifers, dinoflagellates, coccolithophores
Surface-water salinity	16–20‰	17–22‰ (TL-1, ZL-4) 17–25‰ (SL-3) 25–30‰ (JL-2)	Planktonic foraminifers, coccolithophores
Isolation from the ocean	YES	YES	$\delta^{18}O_{carb}$, $^{87}Sr/^{86}Sr_{carb}$, $\delta^{34}S$ of FP
High productivity	YES	YES	TOC, $\delta^{13}C_{org}$, $\delta^{15}N_{org}$, abundance of coccoliths, dinoflagellates
Methane venting	YES	YES (only TL-1)	$\delta^{13}C_{org}$, $\delta^{13}C_{carb}$

5.5. Methane venting

Among all four Oligocene coccolith limestone horizons, TL-1 is distinctive in many aspects. Some data discussed above indicate that TL-1 was deposited in a basin with lower salinity than the other horizons and exceptionally thick anoxic bottom water column that enhanced preservations of OM with exceptionally low $\delta^{15}N_{org}$ values. Its stable carbon isotope composition is also clearly distinct, as both carbonate and organic matter are significantly depleted in ^{13}C (by ~2‰) relative to the other horizons (Fig. 7). This difference cannot account for temporal changes of seawater $\delta^{13}C$, as the global marine $\delta^{13}C$ curve records only small variations < 0.5‰ during the period when the coccolith limestones accumulated (Fig. 2) (Zachos et al., 2001). The $\delta^{13}C_{carb}$ values of the limestones chiefly represent isotopic composition of dissolved inorganic carbon (DIC) in the photic zone, as discussed in 5.3. Therefore, the low $\delta^{13}C$ values of TL-1 indicate that DIC pool was ^{13}C-depleted relative to ambient ocean water during the deposition of this horizon. Such effect was possible, because the basin was restricted and there was little water exchange with the open ocean, which would otherwise buffer any isotopic departure from marine signature.

TL-1 is the oldest coccolith limestone horizon in the Oligocene strata of the Outer Carpathians and was deposited in the middle part of NP23 zone. Interestingly, methane-derived carbonates identified and described by Bojanowski (2007, 2012) from the Fore-Magura unit (equivalent to the Dukla unit) in the Polish Outer Carpathians are of the same age (Barski and Bojanowski, 2010). They precipitated due to anaerobic oxidation of biogenic methane that was produced from organic carbon-rich Eocene-Oligocene sediments (Bojanowski, 2014). Methane was temporarily bound in clathrates which accumulated within the sediments under the basin floor (Bojanowski et al., 2015). Dissociation of methane clathrates liberated large amounts of methane that was being oxidized in the sediments (Bojanowski, 2012) and also vented into the water column (Bojanowski, 2007).

Biogenic methane is extremely depleted in ^{13}C (Claypool and Kaplan, 1974), so DIC produced by oxidation of biogenic methane exhibits extremely low $\delta^{13}C$ of down to −110‰ (Whiticar et al., 1986). Therefore, the presence of large amounts of methane being oxidized in the water column could have caused an overall decrease of $\delta^{13}C$ value of DIC pool in the basin. The ^{13}C-depleted DIC must have also lowered the stable C isotope composition of biomass synthesized in the water column, e.g. primary producers, which likely explains the low $\delta^{13}C_{org}$ values in TL-1 and the associated mudstones. This is supported by hopanoid biomarkers derived from methanotrophic bacteria with very low $\delta^{13}C$ values (≤−40‰) that were identified in the Oligocene deposits of the Polish Outer Carpathians (Köster et al., 1998b). Moreover, molecular and isotopic evidence of methanotrophy in the water column has been also preserved in the adjacent parts of the Paratethys, i.e. in the Hungarian Paleogene Basin (Bechtel et al., 2012) and the Alpine Molasse Basin in Austria (Schulz et al., 2005). This indicates that methane venting and its anaerobic oxidation occurred on a basin-wide scale in the Central Paratethys, similar to the present-day Black Sea, as indicated by strongly ^{13}C-depleted compounds in sinking particulate OM (Schouten et al., 2001; Wakeham et al., 2003), presence of methane-derived seep carbonates occurring on the seafloor (Peckmann et al., 2001; Thiel et al., 2001; Michaelis et al., 2002) and by large methane plumes extending in the water column (Peckmann et al., 2001; Stewart et al., 2007). Therefore, conditions in the Central Paratethys were especially analogous to those in present-day Black Sea during deposition of TL-1 (Table 2), which can be regarded as the closest counterpart of recent sediments in the Black Sea.

6. Conclusions

The Black Sea is a remnant basin of the Paratethys. Biotic, sedimentological and geochemical properties of the Oligocene pelagic coccolith limestones were used to reconstruct paleoceanographic setting of the Central Paratethys during Oligocene and were compared with those of the laminated coccolith marls being currently deposited in the Black Sea. This showed that during Oligocene the Central Paratethys experienced strikingly similar conditions to those that have existed in the Black Sea for most of Holocene, which is synthesized in Table 2:

i. The limestones formed when strong water-column stratification existed in the Paratethys. Bottom-water anoxia was recorded by uniform and small sizes of pyrite framboids having low $\delta^{34}S$, the presence of 28,30-dinorhopane and low-diversity dinoflagellate assemblage with *Homotryblium* spp., absence of benthic organisms or trace fossils and fine primary horizontal lamination of the limestones.
ii. Low salinity conditions in the upper water column caused enrichments in ^{16}O and ^{87}Sr isotopes, waning or disappearance of planktonic foraminifera and massive blooms of low-diversity coccolithophorid assemblages and goniodomid dinoflagellates in the basin. These conditions developed due to limited water exchange with the open ocean, significant riverine flux and enhanced organic sedimentation. Occassionally, the input of seawater was so effectively blocked and the influx of meteoric water so strong that sulfate became almost exhausted in the water column by bacterial sulfate reduction.
iii. Tectonic uplift associated with the orogenic movements and/or eustatic sea level falls at ca. 31.5 and 28.5 Ma were probably responsible for the closure or significant restriction of the straits connecting the basin with the open ocean.
iv. The most extreme conditions occurred during NP23, when anoxic conditions reached exceptionally high in the water column, productivity was particularly enhanced in the surface waters and widespread methane venting occurred. All these processes take place in the Black Sea today as well. The only difference discovered is that euxinic conditions likely did not reach the photic zone in the Paratethys. These similarities indicate that the Tylawa horizon that formed during NP23 should be considered as the best fossil

counterpart of the recent Black Sea sediments.

Thus, using the present-day conditions in the Black Sea as an analogue for evaluating of the Central Paratethyan paleoenvironment during the Oligocene is acceptable, but especially justified for the NP23 zone. Moreover, the Tylawa horizon provides a prediction to how postdepositional processes can modify the properties of a coccolith ooze like the one that has been accumulating in the Black Sea since 2.7 ka.

Acknowledgments

We are grateful to Gert-Jan Reichart (Utrecht University) for his supervision during A. Ciurej research stay at Utrecht. Anchelique Mets (NIOZ) is thanked for analytical support with the organic geochemical analysis. This work was supported by the National Science Centre (grant no. 2011/01/D/ST10/04617) and by the Ministry of Science and Higher Education (grant no. N N307 2744 33). P.K.B. acknowledges funding through NWO-ALW VENI grant no. 863.13.002. S.S. was supported by the Netherlands Earth Science Center, funded by Ministry of Education, Culture and Science, Netherlands (OCW; grant no. NWO 024.002.001). AC, JT and MB were partly supported by the EU 7FP ATLAB Project no. 285989 coordinated by ING PAN. We appreciate constructive comments on the earlier version of the manuscript by Stephen Barker (Cardiff University).

Appendix A. Supplementary data

Supplementary data to this article can be found online at https://doi.org/10.1016/j.margeo.2018.06.011.

References

Alve, E., 1999. Colonization of new habitats by benthic foraminifera: a review. Earth Sci. Rev. 46, 167–185.
Anderson, O.R., Bé, A.W.H., 1976. A cytochemical fine structure study of phagotrophy in a planktonic foraminifer *Hastigerina pelagica* (d'Orbigny). Biol. Bull. 151, 437–449.
Arthur, M.A., Dean, W.E., 1998. Organic-matter production and preservation and evolution of anoxia in the Holocene Black Sea. Paleoceanography 13, 395–411.
Bąk, K., 1999. Late Oligocene foraminifera from the Krosno Beds in the San valley section (Bieszczady Mountains); Silesian unit, Polish Outer Carpathians. Ann. Soc. Geol. Pol. 69, 195–217.
Bąk, K., 2005. Foraminiferal biostratigraphy of the Egerian Flysch sediments in The Silesian Nappe, Outer Carpathians, Polish part of the Bieszczady Mountains. Ann. Soc. Geol. Pol. 75, 71–93.
Báldi, T., 1984. The terminal Eocene and Early Oligocene events in Hungary and the separation of an anoxic, cold Paratethys. Eclogae Geologicae Helvetiae 77, 1–27.
Banner, J.L., 1995. Application of the trace element and isotope geochemistry of strontium to studies of carbonate diagenesis. Sedimentology 42, 805–824.
Barski, M., Bojanowski, M.J., 2010. Organic-walled dinoflagellate cysts as a tool to recognize carbonate concretions: an example from Oligocene flysch deposits of the Western Carpathians. Geol. Carpath. 61, 121–128.
Bathurst, R.G.C., 1981. Carbonate Sediments and Their Diagenesis. Elsevier, Amsterdam.
Bechtel, A., Hámor-Vidó, M., Gratzer, R., Sachsenhofer, R.F., Püttmann, W., 2012. Facies evolution and stratigraphic correlation in the early Oligocene Tard Clay of Hungary as revealed by maceral, biomarker and stable isotope composition. Mar. Pet. Geol. 35, 55–74.
Bennett, R.H., O'Brien, N.R., Hulbert, M.H., 1991. Determinants of clay and shale microfabric signatures: process and mechanisms. In: Bennet, R.H., O'Brien, N.R., Hulbert, M.H. (Eds.), Microstructure of Fine-Grained Sediments. Springer, Berlin, Heidelberg, New York, pp. 5–32.
Berner, R.A., 1969. The synthesis of framboidal pyrite. Econ. Geol. 64, 383–384.
Bieńkowska, M., 2004. Taphonomy of ichthyofauna from an Oligocene sequence (Tylawa Limestones horizon) of the Outer Carpathians, Poland. Geological Quarterly 48, 181–192.
Bieńkowska-Wasiluk, M., 2010. Taphonomy of Oligocene teleost fishes from the Outer Carpathians of Poland. Acta Geol. Pol. 60, 479–533.
Bijma, J., Faber, W.W., Hemleben, C., 1990. Temperature and salinity limits for growth and survival of some planktonic foraminifers in laboratory cultures. J. Foraminifer. Res. 20, 95–116.
Bojanowski, M.J., 2007. Oligocene cold-seep carbonates from the Carpathians and their inferred relation to gas hydrates. Facies 53, 347–360.
Bojanowski, M.J., 2012. Geochemical paleogradient in pore waters controlled by AOM recorded in an Oligocene laminated limestone from the Outer Carpathians. Chem. Geol. 292–293, 45–56.
Bojanowski, M.J., 2014. Authigenic dolomites in the Eocene–Oligocene organic carbon-rich shales from the Polish Outer Carpathians: evidence of past gas production and possible gas hydrate formation in the Silesian basin. Mar. Pet. Geol. 51, 117–135.
Bojanowski, M.J., Bagiński, B., Guillermier, C., Franchi, I.A., 2015. Carbon and oxygen isotope analysis of hydrate-associated Oligocene authigenic carbonates using NanoSIMS and IRMS. Chem. Geol. 416, 51–64.
Bojanowski, M.J., Barczuk, A., Wetzel, A., 2014. Deep-burial alteration of early-diagenetic carbonate concretions formed in Palaeozoic deep-marine greywackes and mudstones (Bardo Unit, Sudetes Mountains, Poland). Sedimentology 61, 1211–1239.
Bojanowski, M.J., Dubicka, Z., Minoletti, F., Olszewska-Nejbert, D., Surowski, M., 2017. Stable C and O isotopic study of the Campanian chalk from the Mielnik section (eastern Poland): signals from bulk rock, belemnites, benthic foraminifera, nannofossils and microcrystalline cements. Palaeogeogr. Palaeoclimatol. Palaeoecol. 465, 193–211.
Boon, J.J., Rijpstra, W.I.C., De Lange, F., et al., 1979. The Black Sea sterol—a molecular fossil for dinoflagellate blooms. Nature 277, 125–127.
Böttcher, M.E., Lepland, A., 2000. Biogeochemistry of sulfur in a sediment core from the west-central Baltic Sea: Evidence from stable isotopes and pyrite textures. J. Mar. Syst. 25, 299–312.
Böttcher, M.E., Thamdrup, B.B., Vennemann, T.W., 2001. Oxygen and sulfur isotope fractionation during anaerobic bacterial disproportionation of elemental sulfur. Geochim. Cosmochim. Acta 65, 1601–1609.
Bottrell, S.H., Newton, R.J., 2006. Reconstruction of changes in global sulfur cycling from marine sulfate isotopes. Earth Sci. Rev. 75, 59–83.
Bottrell, S.H., Raiswell, R., 2000. Sulphur isotopes and microbial sulphur cycling in sediments. In: Riding, R.E., Awramik, S.M. (Eds.), Microbial Sediments. Springer-Verlag, Berlin, pp. 96–104.
Brandes, J.A., Devol, A.H., Yoshinari, T., Jayakumar, D.A., Naqvi, S.W.A., 1998. Isotopic composition of nitrate in the central Arabian Sea and eastern tropical North Pacific: a tracer for mixing and nitrogen cycles. Limnol. Oceanogr. 43, 1680–1689.
Bruch, A.A., 1998. Palynologische Untersuchungen im Oligozän Sloweniens: Paläo-Umwelt und Paläoklima im Ostalpenraum. Tübinger Mikropaläontologische Mitteilungen 18, 1–193.
Burdige, D.J., 2006. Geochemistry of Marine Sediments. Princeton University Press, Princeton.
Calvert, S.E., Karlin, R.E., 1998. Organic carbon accumulation in the Holocene sapropel of the Black Sea. Geology 26, 107–110.
Calvert, S.E., Thode, H.G., Yeung, D., Karlin, R.E., 1996. A stable isotope study of pyrite formation in the Late Pleistocene and Holocene sediments of the Black Sea. Geochim. Cosmochim. Acta 60, 1261–1270.
Canfield, D.E., 2001. Isotope fractionation by natural populations of sulfate-reducing bacteria. Geochim. Cosmochim. Acta 65, 1117–1124.
Canfield, D.E., Raiswell, R., Westrich, J.T., Reaves, C.M., Berner, R.A., 1986. The use of chromium reduction in the analysis of reduced inorganic sulfur in sediments and shales. Chem. Geol. 54, 149–155.
Canfield, D.E., Thamdrup, B., 1994. The production of S-34-depleted sulfide during bacterial disproportionation of elemental sulfur. Science 266 (5193), 1973–1975.
Chambers, L.A., Trudinger, P.A., 1979. Microbiological fractionation of stable sulfur isotopes: a review and critique. Geomicrobiol J. 1, 249–293.
Chambers, L.A., Trudinger, P.A., Smith, J.W., Burns, M.S., 1975. Fractionation of sulfur isotopes by continuous cultures of *Desulfovibrio desulfuricans*. Can. J. Microbiol. 21, 1602–1607.
Ciurej, A., 2009. Procesy i warunki sedymentacji wapieni tylawskich w oligocenie Karpat zewnętrznych (ze szczególnym uwzględnieniem polskiej części Karpat). Ph.D. Thesis. Akademia Górniczo-Hutnicza, AGH, Kraków, pp. 226. available at. http://winntbg.bg.agh.edu.pl/rozprawy2/10220/full10220.pdf.
Ciurej, A., 2010. Procedures for obtaining optimal SEM images of coccolithophore debris in coccolith limestones. Acta Palaeontol. Pol. 55, 169–171.
Ciurej, A., Haczewski, G., 2012. The Tylawa Limestones – a regional marker horizon in the Lower Oligocene of the Paratethys: diagnostic characteristics from the type area. Geol. Quart. 56, 833–844.
Ciurej, A., Haczewski, G., 2016. The Sokoliska Limestone – a new regional marker horizon of coccolith laminites in the Oligocene of the Outer Carpathians: diagnostic features and stratigraphic position. Ann. Soc. Geol. Pol. 86, 415–427.
Claypool, G.E., Kaplan, I.R., 1974. The origin and distribution of methane in marine sediments, in Natural Gases. In: Kaplan, I.R. (Ed.), Marine Sediments. Plenum Press, New York, pp. 99–139.
Çoban-Yıldız, Y., Altabet, M.A., Yılmaz, A., Tuğrul, S., 2006. Carbon and nitrogen isotopic ratios of suspended particulate organic matter (SPOM) in the Black Sea water column. Deep-Sea Res. II 53, 1875–1892.
Codispoti, L.A., Friederich, G.E., Murray, J.W., Sakamoto, C.M., 1991. Chemical variability in the Black Sea: implications of continuous vertical profiles that penetrated the oxic–anoxic interface. Deep-Sea Res. 38, S691–S710.
Cramer, B.S., Toggweiler, J.R., Wright, J.D., Katz, M.E., Miller, K.G., 2009. Ocean overturning since the Late Cretaceous: Inferences from a new benthic foraminiferal isotope compilation. Paleoceanography 24, PA4216.
Detmers, J., Brüchert, V., Habicht, K.S., Kuever, J., 2001. Diversity of sulfur isotope fractionations by sulfate-reducing prokaryotes. Appl. Environ. Microbiol. 67, 888–894.
Dopieralska, J., 2003. Neodymium Isotopic Composition of Conodonts as a Palaeoceanographic Proxy in the Variscan Oceanic System. Ph.D. thesis Justus-Liebig-University, Giessen, pp. 111. available at: http://geb.uni-giessen.de/geb/volltexte/2003/1168/.
Eglinton, G., Hamilton, R.J., 1963. The distribution of alkanes. In: Swain, T. (Ed.), Chemical Plant Taxonomy. Academic Press, London, pp. 187–217.
Eker-Develi, E., Kideys, A.E., 2003. Distribution of phytoplankton in the southern Black Sea in summer 1996, spring and autumn 1998. J. Mar. Syst. 39, 203–211.
Fensome, R.A., Williams, G.L., 2004. The Lentin and Williams Index of Fossil

Dinoflagellates (2004 Edition). American Association of Stratigraphic Palynologists Foundation Contribution Series.
Fry, B., Jannasch, H.W., Molyneaux, S.J., Wirsen, C.O., Muramoto, J.A., King, S., 1991. Stable isotope studies of the carbon, nitrogen and sulfur cycles in the Black Sea and the Cariaco Trench. In: Deep Sea Research Part A. Oceanographic Research Papers 38, Supplement 2, pp. S1003–S1019.
Ganeshram, R.S., Pedersen, T.F., Calvert, S.E., McNeill, G.W., Fonugne, M.R., 2000. Glacial–interglacial variability in denitrification in the world's oceans: causes and consequences. Paleoceanography 15, 361–376.
Gedl, P., 2000. Biostratigraphy and palaeoenvironment of the Podhale Palaeogene (Inner Carpathians, Poland) in the light of palynological studies. Part II. Summary and systematic descriptions. Studia Geol. Polon. 117, 155–303.
Goldberg, T., Poulton, S.W., Strauss, H., 2005. Sulphur and oxygen isotope signatures of late Neoproterozoic to early Cambrian sulphate, Yangtze Platform, China: diagenetic constraints and seawater evolution. Precambrian Res. 137, 223–241.
Gomes, M.L., Hurtgen, M.T., 2015. Sulfur isotope fractionation in modern euxinic systems: implications for paleoenvironmental reconstructions of paired sulfate-sulfide isotope records. Geochim. Cosmochim. Acta 157, 39–55.
Gradstein, F.M., Ogg, J.G., Schmitz, M., Ogg, G., 2012. The Geologic Time Scale. Elsevier Publ. Co, Amsterdam.
Grantham, P.J., Posthuma, J., de Groot, K., 1980. Variation and significance of the C_{27} and C_{28} triterpane content of a North Sea core and various North Sea crude oils. In: Douglas, A.G., Maxwell, J.R. (Eds.), Advances in Organic Geochemistry. Pergamon Press, Oxford, pp. 29–48.
Grassineau, N.V., Mattey, D.P., Lowry, D., 2001. Sulfur isotope analysis of sulfide and sulfate minerals by continuous flow-isotope ratio mass spectrometry. Anal. Chem. 73, 220–225.
Habicht, K.S., Canfield, D.E., 2001. Isotope fractionation by sulfate-reducing natural populations and the isotopic composition of sulfide in marine sediments. Geology 29, 555–558.
Habicht, K.S., Canfield, D.E., Rethmeier, J., 1998. Sulfur isotope fractionation during bacterial reduction and disproportionation of thiosulfate and sulphite. Geochim. Cosmochim. Acta 62, 2585–2595.
Haczewski, G., 1989. Coccolith limestone horizons in the Menilite-Krosno Series (Oligocene, Carpathians): identification, correlation, and origin. Ann. Soc. Geol. Pol. 59, 435–523 (in Polish, summary in English).
Haczewski, G., 1996. Oligocene laminated limestones as a high-resolution correlator of palaeoseismicity, Polish Carpathians. In: Kemp, A.E.S. (Ed.), Palaeoclimatology and Palaeoceanography from Laminated Sediments. Vol. 116. Geological Society Special Publications, pp. 209–220.
Haq, B.U., Al-Qahtani, A.M., 2005. Phanerozoic cycles of sea-level change on the Arabian Platform. GeoArabia 10, 127–160.
Haug, G.H., Pedersen, T.F., Sigman, D.M., Calvert, S.E., Nielsen, B., Peterson, L.C., 1998. Glacial/interglacial variations in production and nitrogen fixation in the Cariaco Basin during the last 580 kyr. Paleoceanography 13, 427–432.
Hemleben, C., Spindler, M., Anderson, O.R., 1989. Modern Planktonic Foraminifera. Springer, New York.
Honjo, S., Roman, M.R., 1978. Marine copepod faecel pellets: production and sedimentation. J. Mar. Res. 36, 45–57.
Huang, Y., Freeman, K.H., Wilkin, R.T., Arthur, M.A., Jones, A.D., 2000. Black Sea chemocline oscillations during the Holocene: molecular and isotopic studies of marginal sediments. Org. Geochem. 31, 1525–1531.
Jensen, M.M., Kuypers, M.M.M., Laviket, G., Thamdrup, B., 2008. Rates and regulation of anaerobic ammonium oxidation and denitrification in the Black Sea. Limnol. Oceanogr. 53, 23–36.
Jones, G.A., Gagnon, A.R., 1994. Radiocarbon chronology of Black Sea sediments. Deep-Sea Res. 41, 531–557.
Jørgensen, B.B., 1982. Mineralization af organic matter in the sea bed - the role of sulphate reduction. Nature 296, 643–645.
Jørgensen, B.B., Böttcher, M.E., Lüschen, H., Neretin, L.N., Volkov, I.I., 2004. Anaerobic methane oxidation and a deep H_2S sink generate isotopically heavy sulfides in Black Sea sediments. Geochim. Cosmochim. Acta 68, 2095–2118.
Jucha, S., 1969. Les schistes de Jasło, leur importance pour la stratigraphie et la sédimentologie de la série ménilitique et des couches de Krosno (Carpathes flyscheuses). Prace Geologiczne, Polska Akademia Nauk-Oddział w Krakowie, Komisja Nauk Geologicznych 52, 1–128.
Karl, D., Letelier, R., Tupas, L., Dore, J., Christian, J., Hebel, D., 1997. The role of nitrogen fixation in biogeochemical cycling in the subtropical North Pacific Ocean. Nature 388, 533–538.
Kominz, M.A., Browning, J.V., Miller, K.G., Sugarman, P.J., Mizintseva, S., Scotese, C.R., 2008. Late Cretaceous to Miocene sea-level estimates from the New Jersey and Delaware coastal plain boreholes: an error analysis. Basin Res. 20, 211–226.
Koopmans, M.P., Köster, J., van Kaam-Peters, H.M.E., Kenig, F., Schouten, S., Hartgers, W.A., de Leeuw, J.W., Sinninghe Damsté, J.S., 1996. Diagenetic and catagenetic products of isorenieratene: Molecular indicators for photic zone anoxia. Geochim. Cosmochim. Acta 60, 4467–4496.
Koopmans, M.P., Rijpstra, W.I.C., Klapwijk, M.M., de Leeuw, J.W., Lewan, M.D., Sinninghe Damsté, J.S., 1999. A thermal and chemical degradation approach to decipher pristane and phytane precursors in sedimentary organic matter. Org. Geochem. 30, 1089–1104.
Koopmans, M.P., Schaeffer-Reiss, C., de Leeuw, J.W., Lewan, M.D., Maxwell, J.R., Schaeffer, P., Sinninghe Damsté, J.S., 1997. Sulphur and oxygen sequestration of n-C_{37} and n-C_{38} unsaturated ketones in an immature kerogen and the release of their carbon skeletons during early stages of thermal maturation. Geochim. Cosmochim. Acta 61, 2397–2408.
Köster, J., Kotarba, M., Lafargue, E., Kosakowski, P., 1998a. Source rock habitat and hydrocarbon potential of Oligocene Menilite Formation (Flysch Carpathians, Southeast Poland): an organic geochemical and isotope approach. Org. Geochem. 29, 543–558.
Köster, J., Rospondek, M., Schouten, S., Kotarba, M., Zubrzycki, A., Sinninghe Damsté, J.S., 1998b. Biomarker geochemistry of a foreland basin: the Oligocene Menilite Formation in the Flysch Carpathians of Southeast Poland. Org. Geochem. 29, 649–669.
Koszarski, L., Żytko, K., 1961. Jasło shales within the Menilite-Krosno Series in the Middle Carpathians. Biul. Inst. Geol. 166, 87–232 (in Polish, summary in English).
Kotarba, M.J., Koltun, Y.V., 2006. The origin and habitat of hydrocarbons of the Polish and Ukrainian parts of the Carpathian province. In: Golonka, J., Picha, F.J. (Eds.), The Carpathians and their Foreland: Geology and Hydrocarbon Resources: AAPG Memoir #84, pp. 395–442.
Kotlarczyk, J., Jerzmańska, A., Świdnicka, E., Wiszniowska, T., 2006. A framework of ichthyofaunal ecostratigraphy of the Oligocene–Early Miocene strata of the Polish Outer Carpathian basin. Ann. Soc. Geol. Pol. 76, 1–111.
Kotlarczyk, J., Uchman, A., 2012. Integrated ichnology and ichthyology of the Oligocene Menilite Formation, Skole and Subsilesian nappes, Polish Carpathians: a proxy to oxygenation history. Palaeogeogr. Palaeoclimatol. Palaeoecol. 331–332, 104–118.
Kováč, M., Nagymarosy, A., Oszczypko, N., Ślączka, A., Csontos, L., Marunteanu, M., Matenco, L., Marton, E., 1998. Palinspastic reconstruction of the Carpathian-Pannonian region during the Miocene. In: Rakus, M. (Ed.), Geodynamic Development of the Western Carpathias. Slovak Geological Survey, Bratislava, pp. 189–217.
Kováč, M., Plašienka, D., Soták, J., Vojtko, R., Oszczypko, N., Less, G., Ćosović, V., Fügenschuh, B., Králiková, S., 2016. Paleogene palaeogeography and basin evolution of the Western Carpathians, Northern Pannonian domain and adjoining areas. Glob. Planet. Chang. 140, 9–27.
Kováč, M., Hudáčková, N., Halásová, E., Kováčová, M., Holcová, K., Oszczypko-Clowes, M., ... Klučiar, T., 2017. The Central Paratethys palaeoceanography: a water circulation model based on microfossil proxies, climate, and changes of depositional environment. Acta Geol. Slov. 9 (2), 75–114.
Krhovský, J., 1981. Microbiostratigraphic correlations in the Outer Flysch Units of the southern Moravia and influence of the eustacy on their paleoeographical development. Zemni Plyn a Nafta 26, 665–688 (in Czech, summary in English).
Krhovský, J., Adamová, J., Hladíková, J., Maslowská, H., 1992. Paleoenvironmental changes across the Eocene/Oligocene boundary in the Ždanice and Pouzdrany Units (Western Carpathians, Czechoslovakia): the long-term trend and orbitally forced changes in calcareous nannofossil assemblages. In: Hamršmíd, B., Young, J.R. (Eds.), Nannoplankton Research. Proceedings of the Fourth INA Conference, Knihovnička Zemnyho Plynu a Nafty, Prague, vol. 14b2. pp. 105–155.
Kuypers, M.M.M., Sliekers, A.O., Lavik, G., Schmid, M., Jørgensen, B.B., Kuenen, J.G., Sinninghe Damsté, J.S., Strous, M., Jetten, M.S.M., 2003. Anaerobic ammonium oxidation by anammox bacteria in the Black Sea. Nature 422, 608–611.
Kuznetsov, A.B., Semikhatov, M.A., Gorokhov, I.M., 2012. The Sr isotope composition of the world ocean, marginal and inland seas: Implications for the Sr isotope stratigraphy. Stratigr. Geol. Correl. 20, 501–515.
Levin, L.A., Michener, R.H., 2002. Isotopic evidence for chemosynthesis-based nutrition of macrobenthos: The lightness of being at Pacific methane seeps. Limnol. Oceanogr. 47, 1336–1345.
Liu, Z., Pagani, M., Zinniker, D., DeConto, R., Huber, M., Brinkhuis, H., Shah, S.R., Leckie, R.M., Pearson, A., 2009. Global cooling during the Eocene-Oligocene climate transition. Science 323, 1187–1190.
Lyons, T.W., 1991. Upper Holocene sediments of the Black Sea: summary of Leg 4 box cores (1988 Black Sea Oceanographic Expedition). In: Murray, J.W., Izdar, E. (Eds.), Black Sea Oceanography. vol. 4. Kluwer, Boston, MA, pp. 401–441.
Lyons, T.W., 1997. Sulfur isotopic trends and pathways of iron sulfide formation in upper Holocene sediments of the anoxic Black Sea. Geochim. Cosmochim. Acta 61, 3367–3382.
Lyons, T.W., Luepke, J.J., Schreiber, M.E., Zieg, G.A., 2000. Sulfur geochemical constraints on Mesoproterozoic restricted marine deposition: lower Belt Supergroup, northwestern United States. Geochim. Cosmochim. Acta 64, 427–437.
Major, C.O., Goldstein, S.L., Ryan, W.B.F., Lericolais, G., Piotrowski, A.M., Hajdas, I., 2006. The co-evolution of Black Sea level and composition through the last deglaciation and its paleoclimatic significance. Quat. Sci. Rev. 25, 2031–2047.
Martini, E., 1971. In: Farinacci, A. (Ed.), Standard Tertiary and Quaternary Calcareous Nannoplankton Zonation. Proceedings of the II Planktonic Conference, Roma, 1970, Tecnoscienza, Romepp. 739–785.
McArthur, J.M., Howarth, R.J., Shields, G.A., 2012. Strontium isotope stratigraphy. et al. In: Gradstein, F.M. (Ed.), The Geologic Time Scale 2012. Elsevier, Amsterdam.
Melinte, M.C., 2005. Oligocene palaeoenvironmental changes in the Romanian Carpathians, revealed by calcareous nannofossils. In: Tyszka, J., Oliwkiewicz-Miklasińska, M., Gedl, P., Kamiński, M. (Eds.), Methods and Applications in Micropalaeontology. Studia Geol. Polon. 124. pp. 341–352.
Meyers, P.A., 1994. Organic geochemical proxies of paleoceanographic, paleolimnologic, and paleoclimatic processes. Org. Geochem. 27, 213–250.
Michaelis, W., Seifert, R., Nauhaus, K., Treude, T., Thiel, V., Blumenberg, M., Knittel, K., Gieseke, A., Peterknecht, K., Pape, T., Boetius, A., Amann, R., Jørgensen, B.B., Widdel, F., Peckmann, J., Pimenov, N.V., Gulin, M.B., 2002. Microbial reefs in the Black Sea fueled by anaerobic oxidation of methane. Science 297, 1013–1015.
Miller, K.G., Kominz, M.A., Browning, J.V., Wright, J.D., Mountain, G.S., Katz, M.E., Sugarman, P.J., Cramer, B.S., Christie-Blick, N., Pekar, S.F., 2005. The Phanerozoic record of global sea-level change. Science 310, 1293–1298.
Miller, K.G., Wright, J.D., Fairbanks, R.G., 1991. Unlocking the ice house: Oligocene-Miocene oxygen isotopes, eustasy, and margin erosion. J. Geophys. Res. 96, 6829–6848.
Möbius, J., Lahajnar, N., Emeiset, K.-C., 2010. Diagenetic control of nitrogen isotope

ratios in Holocene sapropels and recent sediments from the Eastern Mediterranean Sea. Biogeosciences 7, 3901–3914.
Muramoto, J.A., Honjo, S., Fry, B., Hay, B.J., Howarth, R.W., Cisne, J.L., 1991. Sulfur, iron and organic carbon fluxes in the Black Sea: sulfur isotopic evidence for origin of sulfur fluxes. Deep Sea Research Part A. Oceanographic Research Papers 38, S1151–S1187.
Murray, J.W., Jannash, H.W., Honjo, S., Anderson, R.F., Reeburg, W.S., Top, Z., Friederich, G.E., Codispoti, L.A., Izdar, E., 1989. Unexpected changes in the oxic/anoxic interface in the Black Sea. Nature 338, 411–413.
Neretin, L.N., Böttcher, M.E., Grinenko, V.E., 2003. Sulfur isotope geochemistry of the Black Sea water column. Chem. Geol. 200, 59–69.
Olszewska, B., 1984. Kilka uwag o zespołach otwornic towarzyszących wapieniom jasielskim w polskich Karpatach zewnętrznych. (Some remarks on accompanying foraminifer assemblages in Jasło limestones in the Polish Outer Carpathians). Geol. Quart. 28, 689–700.
Olszewska, B., 1998. The Oligocene of the Polish Carpathians. In: Cicha, I., Rögl, F., Rupp, C., Čtyroká, J. (Eds.), Oligocene—Miocene Foraminifera of the Central Paratethys. Abhandlungen der Senckenbergischen Naturforschenden Gesellschaft. vol. 549. pp. 23–28.
Oslick, J.S., Miller, K.G., Feigenson, M.D., 1994. Oligocene-Miocene strontium isotopes: Stratigraphic revisions and correlations to an inferred glacioeustatic record. Paleoceanography 9, 427–443.
Owens, N.J.P., 1987. Marine variation in ^{15}N. Adv. Mar. Biol. 24, 390–451.
Özsoy, E., Ünlüata, Ü., 1997. Oceanography of the Black Sea: a review of some recent results. Earth Sci. Rev. 42, 231–272.
Pacton, M., Gorin, G.E., Vasconcelos, C., 2011. Amorphous organic matter — experimental data on formation and the role of microbes. Rev. Palaeobot. Palynol. 166, 253–267.
Pawellek, F., Frauenstein, F., Veizer, J., 2002. Hydrochemistry and isotope geochemistry of the upper Danube River. Geochim. Cosmochim. Acta 66, 3839–3854.
Paytan, A., Gray, E.T., Ma, Z., Erhardt, A., Faul, K., 2011. Application of sulphur isotopes for stratigraphic correlation. Isot. Environ. Health Stud. 48, 195–206.
Peckmann, J., Reimer, A., Luth, U., Hansen, B.T., Heinicke, C., Hoefs, J., Reitner, J., 2001. Methane-derived carbonates and authigenic pyrite from the northwestern Black Sea. Mar. Geol. 177, 129–150.
Pekar, S.F., Christie-Blick, N., Miller, K.G., Komiz, M.A., 2003. Calibrating Oligocene eustasy to oxygen isotope data: eustatic estimates from two-dimensional flexural backstripping from the new Jersey continental margin (USA). Geophys. Res. Abstr. 5, 13–54.
Perch-Nielsen, K., 1985. Cenozoic calcareous nannofossils. In: Bolli, H.M., Saunders, J.B., Perch-Nielsen, K. (Eds.), Plankton Stratigraphy. Cambridge University Press, Cambridge, pp. 427–555.
Peters, K.E., Walters, C.C., Moldowan, J.M., 2005. The Biomarker Guide. 2nd volume. Cambridge Press, New York, NY.
Pin, Ch., Briot, D., Bassin, Ch., Poitrasson, F., 1994. Concomitant separation of strontium and samarium-neodymium for isotopic analysis in silicate samples, based on specific extraction chromatography. Anal. Chim. Acta 298, 209–222.
Pross, J., Schmiedl, G., 2002. Early Oligocene dinoflagellate cysts from the Upper Rhine Graben (SW Germany): paleoenvironmental and paleoclimatic implications. Mar. Micropaleontol. 45, 1–24.
Puglisi, D., Badescu, D., Carbone, S., Corso, S., Franchi, R., Gigliuto, L.G., Loiacono, F., Miclaus, C., Moretti, E., 2006. Stratigraphy, petrography and palaeogeographic significance of the Early Oligocene “menilite facies” of the Tarcău Nappe (Eastern Carpathians, Romania). Acta Geol. Pol. 56, 105–120.
Quan, T.M., Wright, J.D., Falkowski, P.G., 2013. Co-variation of nitrogen isotopes and redox states through glacial–interglacial cycles in the Black Sea. Geochim. Cosmochim. Acta 112, 305–320.
Reeburgh, W.S., Ward, B.B., Whalen, S.C., Sandbeck, K.A., Kilpatrick, K.A., Kerkhof, L.J., 1991. Black Sea methane geochemistry. Deep-Sea Res. 38 (Suppl. 2), S1189–S1210.
Reilly, T.J., Miller, K.G., Feigenson, M.D., 2002. Latest Eocene-earliest Miocene Sr isotopic reference section, Site 522, eastern South Atlantic. Paleoceanography 17, 1046–1055.
Reschke, S., Ittekkot, V., Panin, N., 2002. The nature of organic matter in the Danube River particles and north-western Black Sea sediments. Estuar. Coast. Shelf Sci. 54, 563–574.
Rögl, F., 1998. Palaeogeographic consideration for Mediterranean and Paratethys Seaways (Oligocene to Miocene). Ann. Naturhist. Mus. Wien 99A, 279–310.
Rögl, F., 1999. Dysaerobic bottom waters. Endemism. Marine faunas only in the westernmost part. Geol. Carpath. 50, 339–349.
Roth, P.H., Mullin, M., Berger, W.H., 1975. Coccolith sedimentation by fecal pellets: laboratory experiments and field observations. Geol. Soc. Am. Bull. 86, 1079–1084.
Sachs, J.P., Repeta, D.J., 1999. Oligotrophy and nitrogen fixation during eastern Mediterranean sapropels events. Science 286, 2485–2488.
Schmidt, F., Erdogan, L.T., 1996. Palaeohydrodynamics in exploration. In: Wessely, G., Liebl, W. (Eds.), Oil and Gas in Alpidic Thrustbelts and Basins of Central and Eastern Europe. EAGE Special Publications 5. The Alden Press, Oxford, pp. 255–265.
Schoell, M., McCaffrey, M.A., Fago, F.J., Moldowan, J.M., 1992. Carbon isotopic compositions of 28,30-bisnorhopanes and other biological markers in a Monterey crude oil. Geochim. Cosmochim. Acta 56, 1391–1399.
Schouten, S., Wakeham, S.G., Sinninghe Damsté, J.S., 2001. Evidence for anaerobic methane oxidation by archaea in euxinic waters of the Black Sea. Org. Geochem. 32, 1277–1281.
Schulz, H.M., Bechtel, A., Sachsenhofer, R.F., 2005. The birth of the Paratethys during the Early Oligocene: from Tethys to an ancient Black Sea analogue? Glob. Planet. Chang. 49, 163–176.
Simoneit, B.R.T., 1986. Cyclic terpenoids in the geosphere. In: Johns, R.B. (Ed.), Biological Markers. The Sedimentary Record Elsevier, Amsterdam, pp. 43–99.
Sinninghe Damsté, J.S., Rijpstra, W.I.C., Kock-van Dalen, A.C., de Leeuw, J.W., Schenck, P.A., 1989. Quenching of labile functionalised lipids by inorganic sulphur species: evidence for the formation of sedimentary organic sulphur compounds at the early stages of diagenesis. Geochim. Cosmochim. Acta 53, 1343–1355.
Sinninghe Damsté, J.S., Schouten, S., Volkman, J.K., 2014. C_{27}–C_{30} neohop-13(18)-enes and their saturated and aromatic derivatives in sediments: Indicators for diagenesis and water column stratification. Geochim. Cosmochim. Acta 133, 402–421.
Sinninghe Damsté, J.S., Wakeham, S.G., Kohnen, M.E.L., Hayes, J.M., de Leeuw, J.W., 1993. A 6,000-year sedimentary molecular record of chemocline excursions in the Black Sea. Nature 362, 827–829.
Sluijs, A., Pross, J., Brinkhuis, H., 2005. From greenhouse to icehouse; organic-walled dinoflagellate cysts as paleoenvironmental indicators in the Paleogene. Earth Sci. Rev. 68, 281–315.
Sótak, J., 2010. Paleoenvironmental changes across the Eocene-Oligocene boundary: insights from the Central-Carpathian Paleogene Basin. Geol. Carpath. 61, 393–418.
Spero, H.J., Williams, D.F., 1990. Evidence for seasonal low-salinity surface waters in the Gulf of Mexico over the last 16,000 years. Paleoceanography 5, 963–975.
Steuber, A.M., Pushkar, P., Hetherington, E.A., 1987. A strontium isotopic study of formation waters from the Illinois Basin U.S.A. Appl. Geochem. 2, 477–494.
Stewart, K., Kassakian, S., Krynytzky, M., DiJulio, D., Murray, J.W., 2007. Oxic, suboxic, and anoxic conditions in the Black Sea. In: Yanko-Hombach, V., Gilbert, A.S., Panin, N., Dolukhanov, P.M. (Eds.), The Black Sea Flood Question: Changes in Coastline, Climate, and Human Settlement. Springer, Dordrecht, pp. 1–21.
Summons, R.E., 1993. Biogeochemical cycles: a review of fundamental aspects of organic matter formation, preservation, and composition. In: Engel, M.H., Macko, S.A. (Eds.), Organic Geochemistry - Principles and Applications. Plenum Press, New York, pp. 3–21.
Švábenická, L., Bubík, M., Stráník, Z., 2007. Biostratigraphy and paleoenvironmental changes on the transition from the Menilite to Krosno lithofacies (Western Carpathians, Czech Republic). Geol. Carpath. 58, 237–262.
Sweeney, R.E., Kaplan, I.R., 1973. Pyrite framboid formation: Laboratory synthesis and marine sediments. Econ. Geol. 68, 618–634.
Sweeney, R.E., Kaplan, I.R., 1980. Stable isotope composition of dissolved sulfate and hydrogen sulfide in the Black Sea. Mar. Chem. 9, 145–152.
Tari, G., Báldi, T., Báldi-Beke, M., 1993. Paleogene retroarc flexural basin beneath the Neogene Pannonian Basin: a geodynamic model. Tectonophysics 226, 433–455.
Ten Haven, H.L., de Leeuw, J.W., Rullkötter, J., Sinninghe Damsté, J.S., 1987. Restricted utility of the pristane/phytane ratio as a paleoenvironmental indicator. Nature 330, 641–643.
Thiel, V., Peckmann, J., Richnow, H.H., Luth, U., Reitner, J., Michaelis, W., 2001. Molecular signals for anaerobic methane oxidation in Black Sea seep carbonates and a microbial mat. Mar. Chem. 73, 97–112.
Tremblin, M., Hermoso, M., Minoletti, F., 2016. Equatorial heat accumulation as a long-term trigger of permanent Antarctic ice sheets during the Cenozoic. PNAS 113, 11782–11787.
Tuğrul, S., Baştürk, Ö., Saydam, C., Yılmaz, A., 1992. Changes in the hydrochemistry of the Black Sea inferred from water density profiles. Nature 359, 137–139.
Tuzhilkin, V.S., 2008. Thermohaline structure of the sea. In: Kostianoy, A., Kosarev, A. (Eds.), The Black Sea Environment. The Handbook of Environmental Chemistry. vol. 5. Springer–Verlag, Berlin Heidelberg, pp. 217–254 Part Q.
Vetö, I., 1987. An Oligocene sink for organic carbon: upwelling in the Paratethys. Palaeogeogr. Palaeoclimatol. Palaeoecol. 60, 143–153.
Volkman, J.K., Barrett, S.M., Dunstan, G.A., 1994. C_{25} and C_{30} highly branched isoprenoid alkenes in laboratory cultures of two marine diatoms. Org. Geochem. 21, 407–413.
Wada, E., Hattori, A., 1990. Nitrogen in the Sea: Forms, Abundances, and Rate Processes. CRC Press, Boca Raton, FL.
Wakeham, S.G., Lewis, C.M., Hopmans, E.C., Schouten, S., Sinninghe Damsté, J.S., 2003. Archaea mediate anaerobic oxidation of methane in deep euxinic waters of the Black Sea. Geochim. Cosmochim. Acta 67, 1359–1374.
Westley, M.B., Yamagishi, H., Popp, B.N., Yoshida, N., 2006. Nitrous oxide cycling in the Black Sea inferred from stable isotope and isotopomer distributions. Deep-Sea Res. II 53, 1802–1816.
Whiticar, M.J., Faber, E., Schoell, M., 1986. Biogenic methane formation in marine and freshwater environments: CO_2 reduction vs. acetate fermentation–isotope evidence. Geochim. Cosmochim. Acta 50, 693–709.
Wignall, P.B., Newton, R., 1998. Pyrite framboid diameter as a measure of oxygen deficiency in ancient mudrocks. Am. J. Sci. 298, 537–552.
Wilkin, R.T., Arthur, M.A., 2001. Variations in pyrite texture, sulfur isotope composition, and iron systematics in the Black Sea: Evidence for Late Pleistocene to Holocene excursions of the O_2-H_2S redox transition. Geochim. Cosmochim. Acta 65, 1399–1416.
Wilkin, R.T., Arthur, M.A., Dean, W.E., 1997. History of water-column anoxia in the Black Sea indicated by pyrite framboid size distributions. Earth Planet. Sci. Lett. 148, 517–525.
Wilkin, R.T., Barnes, H.L., 1996. Pyrite formation by reactions of iron monosulfides with dissolved inorganic and organic sulfur species. Geochim. Cosmochim. Acta 60, 4167–4179.
Wilkin, R.T., Barnes, H.L., Brantley, S.L., 1996. The size distribution of framboidal pyrite in modern sediments: an indicator of redox conditions. Geochim. Cosmochim. Acta 60, 3897–3912.
Zaback, D.A., Pratt, L.M., Hayes, J.M., 1993. Transport and reduction of sulfate and immobilization of sulfide in marine black shales. Geology 21, 141–144.
Zachos, J., Pagani, M., Sloan, L., Thomas, E., Billups, K., 2001. Trends, rhythms, and aberrations in global climate 65 Ma to present. Science 292, 686–693.
Zachos, J.C., Lohmann, K.C., Walker, J.C.G., Wise, S.W., 1993. Abrupt climate change and transient climates during the Paleogene: a marine perspective. J. Geol. 101, 191–213.